Additional file 3: Table S3. Predicted target genes for ALS-specific down-regulated miRNAs identified by miRmap web-based open source software.

Additional file 4: Table S4. Gene ontology enrichment analysis (bilogical process) of predicted target genes for disease-specific miRNAs.

Additional file 5: Table S5. Summary of up- or down-regulated miRNAs in ALS.

Competing interests
The authors declare that they have no competing interests.

Authors contributions
JU, HS and KW managed the study and were principally responsible for writing. FM, AK, HT and KW performed the neuropathological observation and evaluation. JU performed bioinformatics analysis. HS and KW supervised whole process of the study. All authors read and approved the final manuscript.

Acknowledgements
The authors wish to express their gratitude to M. Nakata, A. Ono and Y. Hama for technical assistance.

Funding
This work was supported by JSPS KAKENHI Grant Number 26430049 (F.M.) and 24300131 (K.W.), a Grant from Japan Science and Technology Program (AS2314204F) (H.S., K.W.), a Grant for Hirosaki University Institutional Research (K.W.), the Collaborative Research Project (2014 2508) of the Brain Research Institute, Niigata University (F.M.), Grants-in-Aid for Research on rare and intractable diseases, the Research Committee on Establishment of Novel Treatments for Amyotrophic Lateral Sclerosis (H.S.), the Research Committee for Ataxic Disease (H.S., K.W.) and the Research Committee of CNS Degenerative Diseases (H.S.) from the Ministry of Health, Labour and Welfare, Japan, and an Intramural Research Grant (24 5) for Neurological and Psychiatric Disorders of NCNP (K.W.).

Author details
[1]Department of Neuropathology, Institute of Brain Science, Hirosaki University Graduate School of Medicine, 5 Zaifu-cho, Hirosaki 036-8562, Japan. [2]Department of Pathological Neuroscience, Center for Bioresource-based Researches, Brain Research Institute, University of Niigata, Niigata, Japan. [3]Department of Pathology, Brain Research Institute, University of Niigata, Niigata, Japan. [4]Department of Neurology, Hokkaido University Graduate School of Medicine, Sapporo, Japan.

Received: 30 October 2014 Accepted: 1 December 2014
Published online: 14 December 2014

References
1. Bartel DP (2004) MicroRNAs: genomics, biogenesis, mechanism, and function. Cell 116(2):281 297
2. Esquela-Kerscher A, Slack FJ (2006) Oncomirs - microRNAs with a role in cancer. Nat Rev Cancer 6(4):259 269
3. Lewis BP, Burge CB, Bartel DP (2005) Conserved seed pairing, often flanked by adenosines, indicates that thousands of human genes are microRNA targets. Cell 120(1):15 20
4. Ambros V (2004) The functions of animal microRNAs. Nature 431(7006):350 355
5. Ma L, Weinberg RA (2008) Micromanagers of malignancy: role of microRNAs in regulating metastasis. Trends Genet 24(9):448 456
6. Cogswell JP, Ward J, Taylor IA, Waters M, Shi Y, Cannon B, Kelnar K, Kemppainen J, Brown D, Chen C, Prinjha RK, Richardson JC, Saunders AM, Roses AD, Richards CA (2008) Identification of miRNA changes in Alzheimer s disease brain and CSF yields putative biomarkers and insights into disease pathways. J Alzheimer s Dis 14(1):27 41
7. Cui JG, Li YY, Zhao Y, Bhattacharjee S, Lukiw WJ (2010) Differential regulation of interleukin-1 receptor-associated kinase-1 (IRAK-1) and IRAK-2 by microRNA-146a and NF-κB in stressed human astroglial cells and in Alzheimer disease. J Biol Chem 285(50):38951 38960
8. Faghihi MA, Zhang M, Huang J, Modarresi F, Van der Brug MP, Nalls MA, Cookson MR, St-Laurent G 3rd, Wahlestedt C (2010) Evidence for natural antisense transcript-mediated inhibition of microRNA function. Genome Biol 11(5):R56
9. Geekiyanage H, Chan C (2011) MicroRNA-137/181c regulates serine palmitoyltransferase and in turn amyloid β, novel targets in sporadic Alzheimer s disease. J Neurosci 31(41):14820 14830
10. G?tz J, Ittner LM, F?ndrich M, Schonrock N (2008) Is tau aggregation toxic or protective: a sensible question in the absence of sensitive methods? J Alzheimer s Dis 14(4):423 429
11. H?bert SS, Horr? K, Nicola? L, Papadopoulou AS, Mandemakers W, Silahtaroglu AN, Kauppinen S, Delacourte A, De Strooper B (2008) Loss of microRNA cluster miR-29a/b-1 in sporadic Alzheimer s disease correlates with increased BACE1/β-secretase expression. Proc Natl Acad Sci U S A 105(17):6415 6420
12. H?bert SS, Horr? K, Nicola? L, Bergmans B, Papadopoulou AS, Delacourte A, De Strooper B (2009) MicroRNA regulation of Alzheimer s amyloid precursor protein expression. Neurobiol Dis 33(3):422 428
13. H?bert SS, Papadopoulou AS, Smith P, Galas MC, Planel E, Silahtaroglu AN, Sergeant N, Bu?e L, De Strooper B (2010) Genetic ablation of Dicer in adult forebrain neurons results in abnormal tau hyperphosphorylation and neurodegeneration. Hum Mol Genet 19(20):3959 3969
14. Lukiw WJ (2007) Micro-RNA speciation in fetal, adult and Alzheimer s disease hippocampus. Neuroreport 18(3):297 300
15. Lukiw WJ, Zhao Y, Cui JG (2008) An NF-κB-sensitive micro RNA-146a-mediated inflammatory circuit in Alzheimer disease and in stressed human brain cells. J Biol Chem 283(46):31315 31322
16. Nunez-Iglesias J, Liu CC, Morgan TE, Finch CE, Zhou XJ (2010) Joint genome-wide profiling of miRNA and mRNA expression in Alzheimer s disease cortex reveals altered miRNA regulation. PLoS One 5(2):e8898
17. Schratt G (2009) microRNAs at the synapse. Nat Rev Neurosci 10(12):842 849
18. Sethi P, Lukiw WJ (2009) Micro-RNA abundance and stability in human brain: specific alterations in Alzheimer s disease temporal lobe neocortex. Neurosci Lett 459(2):100 104
19. Shioya M, Obayashi S, Tabunoki H, Arima K, Saito Y, Ishida T, Satoh J (2010) Aberrant microRNA expression in the brains of neurodegenerative diseases: miR-29a decreased in Alzheimer disease brains targets neurone navigator 3. Neuropathol Appl Neurobiol 36(4):320 330
20. Smith P, Al Hashimi A, Girard J, Delay C, H?bert SS (2011) In vivo regulation of amyloid precursor protein neuronal splicing by microRNAs. J Neurochem 116(2):240 247
21. Wang WX, Rajeev BW, Stromberg AJ, Ren N, Tang G, Huang Q, Rigoutsos I, Nelson PT (2008) The expression of microRNA miR-107 decreases early in Alzheimer s disease and may accelerate disease progression through regulation of β-site amyloid precursor protein-cleaving enzyme 1. J Neurosci 28(5):1213 1223
22. Wang WX, Huang Q, Hu Y, Stromberg AJ, Nelson PT (2011) Patterns of microRNA expression in normal and early Alzheimer s disease human temporal cortex: white matter versus gray matter. Acta Neuropathol 121(2):193 205
23. Doxakis E (2010) Post-transcriptional regulation of α-synuclein expression by mir-7 and mir-153. J Biol Chem 285(17):12726 12734
24. Gehrke S, Imai Y, Sokol N, Lu B (2010) Pathogenic LRRK2 negatively regulates microRNA-mediated translational repression. Nature 466(7306):637 641
25. Junn E, Lee KW, Jeong BS, Chan TW, Im JY, Mouradian MM (2009) Repression of alpha-synuclein expression and toxicity by microRNA-7. Proc Natl Acad Sci U S A 106(31):13052 13057
26. Kim J, Inoue K, Ishii J, Vanti WB, Voronov SV, Murchison E, Hannon G, Abeliovich A (2007) A microRNA feedback circuit in midbrain dopamine neurons. Science 317(5842):1220 1224
27. Wang G, van der Walt JM, Mayhew G, Li YJ, Z?chner S, Scott WK, Martin ER, Vance JM (2008) Variation in the miRNA-433 binding site of FGF20 confers risk for Parkinson disease by overexpression of α-synuclein. Am J Hum Genet 82(2):283 289
28. Johnson R, Zuccato C, Belyaev ND, Guest DJ, Cattaneo E, Buckley NJ (2008) A microRNA-based gene dysregulation pathway in Huntington s disease. Neurobiol Dis 29(3):438 445
29. Lee ST, Chu K, Im WS, Yoon HJ, Im JY, Park JE, Park KH, Jung KH, Lee SK, Kim M, Roh JK (2011) Altered microRNA regulation in Huntington s disease models. Exp Neurol 227(1):172 179
30. Packer AN, Xing Y, Harper SQ, Jones L, Davidson BL (2008) The bifunctional microRNA miR-9/miR-9* regulates REST and CoREST and is downregulated in Huntington s disease. J Neurosci 28(53):14341 14346
31. Ubhi K, Rockenstein E, Kragh C, Inglis C, Spencer B, Michael S, Mante M, Adame A, Galasko D, Masliah E (2014) Widespread microRNA dysregulation

in multiple system atrophy - disease-related alteration in miR-96. Eur J Neurosci 39(6):1026 1041
32. Bruneteau G, Simonet T, Bauch? S, Mandjee N, Malfatti E, Girard E, Tanguy ML, Behin A, Khiami F, Sariali E, Hell-Remy C, Salachas F, Pradat PF, Fournier E, Lacomblez L, Koenig J, Romero NB, Fontaine B, Meininger V, Schaeffer L, Hanta? D (2013) Muscle histone deacetylase 4 upregulation in amyotrophic lateral sclerosis: potential role in reinnervation ability and disease progression. Brain 136(Pt 8):2359 2368
33. De Felice B, Guida M, Guida M, Coppola C, De Mieri G, Cotrufo R (2012) A miRNA signature in leukocytes from sporadic amyotrophic lateral sclerosis. Gene 508(1):35 40
34. De Felice B, Annunziata A, Fiorentino G, Borra M, Biffali E, Coppola C, Cotrufo R, Brettschneider J, Giordana ML, Dalmay T, Wheeler G, D Alessandro R (2014) miR-338-3p is over-expressed in blood, CFS, serum and spinal cord from sporadic amyotrophic lateral sclerosis patients. Neurogenetics: Epub ahead of print
35. Russell AP, Wada S, Vergani L, Hock MB, Lamon S, L?ger B, Ushida T, Cartoni R, Wadley GD, Hespel P, Kralli A, Soraru G, Angelini C, Akimoto T (2012) Disruption of skeletal muscle mitochondrial network genes and miRNAs in amyotrophic lateral sclerosis. Neurobiol Dis 49C:107 117
36. Williams AH, Valdez G, Moresi V, Qi X, McAnally J, Elliott JL, Bassel-Duby R, Sanes JR, Olson EN (2009) MicroRNA-206 delays ALS progression and promotes regeneration of neuromuscular synapses in mice. Science 326 (5959):1549 1554
37. Freischmidt A, M?ller K, Ludolph AC, Weishaupt JH (2013) Systemic dysregulation of TDP-43 binding microRNAs in amyotrophic lateral sclerosis. Acta Neuropathol Commun 1(1):42
38. Margis R, Margis R, Rieder CR (2011) Identification of blood microRNAs associated to Parkinson s disease. J Biotechnol 152(3):96 101
39. Schipper HM, Maes OC, Chertkow HM, Wang E (2007) MicroRNA expression in Alzheimer blood mononuclear cells. Gene Regul Syst Bio 1:263 274
40. Doleshal M, Magotra AA, Choudhury B, Cannon BD, Labourier E, Szafranska AE (2008) Evaluation and validation of total RNA extraction methods for microRNA expression analyses in formalin-fixed, paraffin-embedded tissues. J Mol Diagn 10(3):203 211
41. Glud M, Klausen M, Gniadecki R, Rossing M, Hastrup N, Nielsen FC, Drzewiecki KT (2009) MicroRNA expression in melanocytic nevi: the usefulness of formalin-fixed, paraffin-embedded material for miRNA microarray profiling. J Invest Dermatol 129(5):1219 1224
42. Lewis F, Maughan NJ, Smith V, Hillan K, Quirke P (2001) Unlocking the archive gene expression in paraffin-embedded tissue. J Pathol 195(1):66 71
43. Liu A, Tetzlaff MT, Vanbelle P, Elder D, Feldman M, Tobias JW, Sepulveda AR, Xu X (2009) MicroRNA expression profiling outperforms mRNA expression profiling in formalin-fixed paraffin-embedded tissues. Int J Clin Exp Pathol 2(6):519 527
44. Szafranska AE, Davison TS, Shingara J, Doleshal M, Riggenbach JA, Morrison CD, Jewell S, Labourier E (2008) Accurate molecular characterization of formalin-fixed, paraffin-embedded tissues by microRNA expression profiling. J Mol Diagn 10(5):415 423
45. Xi Y, Nakajima G, Gavin E, Morris CG, Kudo K, Hayashi K, Ju J (2007) Systematic analysis of microRNA expression of RNA extracted from fresh frozen and formalin-fixed paraffin-embedded samples. RNA 13(10):1668 1674
46. Bing Z, Master SR, Tobias JW, Baldwin DA, Xu XW, Tomaszewski JE (2012) MicroRNA expression profiles of seminoma from paraffin-embedded formalin-fixed tissue. Virchows Arch 461(6):663 668
47. Chen L, Li Y, Fu Y, Peng J, Mo MH, Stamatakos M, Teal CB, Brem RF, Stojadinovic A, Grinkemeyer M, McCaffrey TA, Man YG, Fu SW (2013) Role of deregulated microRNAs in breast cancer progression using FFPE tissue. PLoS One 8(1):e54213
48. Ibusuki M, Fu P, Yamamoto S, Fujiwara S, Yamamoto Y, Honda Y, Iyama K, Iwase H (2013) Establishment of a standardized gene-expression analysis system using formalin-fixed, paraffin-embedded, breast cancer specimens. Breast Cancer 20(2):159 166
49. Lee TS, Jeon HW, Kim YB, Kim YA, Kim MA, Kang SB (2013) Aberrant microRNA expression in endometrial carcinoma using formalin-fixed paraffin-embedded (FFPE) tissues. PLoS One 8(12):e81421
50. Osawa S, Shimada Y, Sekine S, Okumura T, Nagata T, Fukuoka J, Tsukada K (2011) MicroRNA profiling of gastric cancer patients from formalin-fixed paraffin-embedded samples. Oncol Lett 2(4):613 619
51. Penland SK, Keku TO, Torrice C, He X, Krishnamurthy J, Hoadley KA, Woosley JT, Thomas NE, Perou CM, Sandler RS, Sharpless NE (2007) RNA expression analysis of formalin-fixed paraffin-embedded tumors. Lab Invest 87(4):383 391
52. Masuda N, Ohnishi T, Kawamoto S, Monden M, Okubo K (1999) Analysis of chemical modification of RNA from formalin-fixed samples and optimization of molecular biology applications for such samples. Nucleic Acids Res 27(22):4436 4443
53. Vejnar CE, Zdobnov EM (2012) miRmap: Comprehensive prediction of microRNA target repression strength. Nucleic Acids Res 40(22):11673 11683
54. Cowherd RB, Asmar MM, Alderman JM, Alderman EA, Garland AL, Busby WH, Bodnar WM, Rusyn I, Medoff BD, Tisch R, Mayer-Davis E, Swenberg JA, Zeisel SH, Combs TP (2010) Adiponectin lowers glucose production by increasing SOGA. Am J Pathol 177(4):1936 1945
55. Fimia GM, Stoykova A, Romagnoli A, Giunta L, Di Bartolomeo S, Nardacci R, Corazzari M, Fuoco C, Ucar A, Schwartz P, Gruss P, Piacentini M, Chowdhury K, Cecconi F (2007) Ambra1 regulates autophagy and development of the nervous system. Nature 447(7148):1121 1125
56. Zhong Y, Wang QJ, Li X, Yan Y, Backer JM, Chait BT, Heintz N, Yue Z (2009) Distinct regulation of autophagic activity by Atg14L and Rubicon associated with Beclin 1-phosphatidylinositol-3-kinase complex. Nat Cell Biol 11(4):468 476
57. Chan EY, Longatti A, McKnight NC, Tooze SA (2009) Kinase-inactivated ULK proteins inhibit autophagy via their conserved C-terminal domains using an Atg13-independent mechanism. Mol Cell Biol 29(1):157 171
58. Mori F, Tanji K, Miki Y, Wakabayashi K (2009) Decreased cystatin C immunoreactivity in spinal motor neurons and astrocytes in amyotrophic lateral sclerosis. J Neuropathol Exp Neurol 68(11):1200 1206
59. Groelz D, Sobin L, Branton P, Compton C, Wyrich R, Rainen L (2013) Non-formalin fixative versus formalin-fixed tissue: a comparison of histology and RNA quality. Exp Mol Pathol 94(1):188 194
60. von Ahlfen S, Missel A, Bendrat K, Schlumpberger M (2007) Determinants of RNA quality from FFPE samples. PLoS One 2(12):e1261
61. Shi X, Wallis AM, Gerard RD, Voelker KA, Grange RW, DePinho RA, Garry MG, Garry DJ (2012) Foxk1 promotes cell proliferation and represses myogenic differentiation by regulating Foxo4 and Mef2. J Cell Sci 125(Pt 22):5329 5337
62. Liu N, Nelson BR, Bezprozvannaya S, Shelton JM, Richardson JA, Bassel-Duby R, Olson EN (2014) Requirement of MEF2A, C, and D for skeletal muscle regeneration. Proc Natl Acad Sci U S A 111(11):4109 4114
63. Humphries AC, Donnelly SK, Way M (2014) Cdc42 and the Rho GEF intersectin-1 collaborate with Nck to promote N-WASPdependent actin polymerisation. J Cell Sci 127(Pt 3):673 685
64. Tsetsenis T, Younts TJ, Chiu CQ, Kaeser PS, Castillo PE, S?dhof TC (2011) Rab3B protein is required for long-term depression of hippocampal inhibitory synapses and for normal reversal learning. Proc Natl Acad Sci U S A 108(34):14300 14305
65. Carta E, Chung SK, James VM, Robinson A, Gill JL, Remy N, Vanbellinghen JF, Drew CJ, Cagdas S, Cameron D, Cowan FM, Del Toro M, Graham GE, Manzur AY, Masri A, Rivera S, Scalais E, Shiang R, Sinclair K, Stuart CA, Tijssen MA, Wise G, Zuberi SM, Harvey K, Pearce BR, Topf M, Thomas RH, Supplisson S, Rees MI, Harvey RJ (2012) Mutations in the GlyT2 gene (SLC6A5) are a second major cause of startle disease. J Biol Chem 287(34):28975 28985
66. Ajit Bolar N, Vanlander AV, Wilbrecht C, Van der Aa N, Smet J, De Paepe B, Vandeweyer G, Kooy F, Eyskens F, De Latter E, Delanghe G, Govaert P, Leroy JG, Loeys B, Lill R, Van Laer L, Van Coster R (2013) Mutation of the iron-sulfur cluster assembly gene IBA57 causes severe myopathy and encephalopathy. Hum Mol Genet 22(13):2590 2602
67. Rowe GC, Jang C, Patten IS, Arany Z (2011) PGC-1β regulates angiogenesis in skeletal muscle. Am J Physiol Endocrinol Metab 301(1):E155 E163
68. Yang Q, She H, Gearing M, Colla E, Lee M, Shacka JJ, Mao Z (2009) Regulation of neuronal survival factor MEF2D by chaperone-mediated autophagy. Science 323(5910):124 127
69. Francius C, Clotman F (2010) Dynamic expression of the Onecut transcription factors HNF-6, OC-2 and OC-3 during spinal motor neuron development. Neuroscience 165(1):116 129
70. Shen E, Shulha H, Weng Z, Akbarian S (2004) Regulation of histone H3K4 methylation in brain development and disease. Philos Trans R Soc Lond B Biol Sci 369(1652). doi:10.1098/rstb.2013.0514
71. Toriumi K, Ikami M, Kondo M, Mouri A, Koseki T, Ibi D, Furukawa-Hibi Y, Nagai T, Mamiya T, Nitta A, Yamada K, Nabeshima T (2013) SHATI/NAT8L regulates neurite outgrowth via microtubule stabilization. J Neurosci Res 91(12):1525 1532
72. Wilczynska KM, Singh SK, Adams B, Bryan L, Rao RR, Valerie K, Wright S, Griswold-Prenner I, Kordula T (2009) Nuclear factor I isoforms regulate gene expression during the differentiation of human neural progenitors to astrocytes. Stem Cells 27(5):1173 1181

73. Wei J, Fujita M, Nakai M, Waragai M, Watabe K, Akatsu H, Rockenstein E, Masliah E, Hashimoto M (2007) Enhanced lysosomal pathology caused by β-synuclein mutants linked to dementia with Lewy bodies. J Biol Chem 282 (39):28904 28914
74. Wen Y, Zand B, Ozpolat B, Szczepanski MJ, Lu C, Yuca E, Carroll AR, Alpay N, Bartholomeusz C, Tekedereli I, Kang Y, Rupaimoole R, Pecot CV, Dalton HJ, Hernandez A, Lokshin A, Lutgendorf SK, Liu J, Hittelman WN, Chen WY, Lopez-Berestein G, Szajnik M, Ueno NT, Coleman RL, Sood AK (2014) Antagonism of tumoral prolactin receptor promotes autophagy-related cell death. Cell Rep 7(2):488 500
75. Choi AM, Ryter SW, Levine B (2013) Autophagy in human health and disease. N Engl J Med 368(7):651 662
76. Nixon RA, Yang DS (2011) Autophagy failure in Alzheimer s disease locating the primary defect. Neurobiol Dis 43(1):38 45
77. Sasaki S (2011) Autophagy in spinal cord motor neurons in sporadic amyotrophic lateral sclerosis. J Neuropathol Exp Neurol 70(5):349 359
78. Tanji K, Mori F, Kakita A, Takahashi H, Wakabayashi K (2011) Alteration of autophagosomal proteins (LC3, GABARAP and GATE-16) in Lewy body disease. Neurobiol Dis 43(3):690 697
79. Tanji K, Odagiri S, Maruyama A, Mori F, Kakita A, Takahashi H, Wakabayashi K (2012) Alteration of autophagosomal proteins in multiple system atrophy. Neurobiol Dis 49C:190 198
80. Sepe S, Nardacci R, Fanelli F, Rosso P, Bernardi C, Cecconi F, Mastroberardino PG, Piacentini M, Moreno S (2014) Expression of Ambra1 in mouse brain during physiological and Alzheimer type aging. Neurobiol Aging 35(1):96 108
81. Abrahamsen HN, Steiniche T, Nexo E, Hamilton-Dutoit SJ, Sorensen BS (2003) Towards quantitative mRNA analysis in paraffin-embedded tissues using real-time reverse transcriptase-polymerase chain reaction: a methodological study on lymph nodes from melanoma patients. J Mol Diagn 5(1):34 41
82. Peir?-Chova L, Pe?a-Chilet M, L?pez-Guerrero JA, Garc?a-Gim?nez JL, Alonso-Yuste E, Burgues O, Lluch A, Ferrer-Lozano J, Ribas G (2013) High stability of microRNAs in tissue samples of compromised quality. Virchows Arch 463(6):765 774
83. Hui AB, Shi W, Boutros PC, Miller N, Pintilie M, Fyles T, McCready D, Wong D, Gerster K, Waldron L, Jurisica I, Penn LZ, Liu FF (2009) Robust global micro-RNA profiling with formalin-fixed paraffin-embedded breast cancer tissues. Lab Invest 89(5):597 606
84. Hutvagner G, Simard MJ (2008) Argonaute proteins: key players in RNA silencing. Nat Rev Mol Cell Biol 9(1):22 32
85. Mourelatos Z, Dostie J, Paushkin S, Sharma A, Charroux B, Abel L, Rappsilber J, Mann M, Dreyfuss G (2002) miRNPs: a novel class of ribonucleoproteins containing numerous microRNAs. Genes Dev 16(6):720 728
86. Arai T, Hasegawa M, Akiyama H, Ikeda K, Nonaka T, Mori H, Mann D, Tsuchiya K, Yoshida M, Hashizume Y, Oda T (2006) TDP-43 is a component of ubiquitin-positive tau-negative inclusions in frontotemporal lobar degeneration and amyotrophic lateral sclerosis. Biochem Biophys Res Commun 351(3):602 611
87. Neumann M, Sampathu DM, Kwong LK, Truax AC, Micsenyi MC, Chou TT, Bruce J, Schuck T, Grossman M, Clark CM, McCluskey LF, Miller BL, Masliah E, Mackenzie IR, Feldman H, Feiden W, Kretzschmar HA, Trojanowski JQ, Lee VM (2006) Ubiquitinated TDP-43 in frontotemporal lobar degeneration and amyotrophic lateral sclerosis. Science 314(5796):130 133
88. Van Humbeeck C, Cornelissen T, Hofkens H, Mandemakers W, Gevaert K, De Strooper B, Vandenberghe W (2011) Parkin interacts with Ambra1 to induce mitophagy. J Neurosci 31(28):10249 10261
89. Wang IF, Guo BS, Liu YC, Wu CC, Yang CH, Tsai KJ, Shen CK (2012) Autophagy activators rescue and alleviate pathogenesis of a mouse model with proteinopathies of the TAR DNA-binding protein 43. Proc Natl Acad Sci U S A 109(37):15024 15029
90. Zhang X, Li L, Chen S, Yang D, Wang Y, Zhang X, Wang Z, Le W (2011) Rapamycin treatment augments motor neuron degeneration in $SOD1^{G93A}$ mouse model of amyotrophic lateral sclerosis. Autophagy 7(4):412 425

doi:10.1186/s40478-014-0173-z
Cite this article as: Wakabayashi *et al.*: Analysis of microRNA from archived formalin-fixed paraffin-embedded specimens of amyotrophic lateral sclerosis. *Acta Neuropathologica Communications* 2014 2:173.

Brain Pathology ISSN 1015-6305

RESEARCH ARTICLE

p62 Deficiency Enhances α-Synuclein Pathology in Mice

Kunikazu Tanji[1]*; Saori Odagiri[2]*; Yasuo Miki[1]; Atsushi Maruyama[3]; Yoshikazu Nikaido[4]; Junsei Mimura[3]; Fumiaki Mori[1]; Eiji Warabi[5]; Toru Yanagawa[5]; Shinya Ueno[4]; Ken Itoh[3]; Koichi Wakabayashi[1]

[1] Department of Neuropathology, [3] Department of Stress Response Science, [4] Department of Neurophysiology, Hirosaki University Graduate School of Medicine, Hirosaki, [2] Department of Neuroanatomy, Cell Biology and Histology, [5] Majors of Medical Sciences, University of Tsukuba, Tsukuba, Japan.

Keywords
α-synuclein, Lewy body disease, p62/Sequestsome 1/SQSTM1, Parkinson's disease, proteolysis, stress.

Corresponding author:
Kunikazu Tanji, PhD, Department of Neuropathology, Hirosaki University Graduate School of Medicine, 5 Zaifu-cho, Hirosaki 036-8562, Japan
(E-mail: *kunikazu@cc.hirosaki-u.ac.jp*)

Received 16 June 2014
Accepted 02 October 2014
Published Online Article Accepted 10 October 2014

* These authors contributed equally to the manuscript.

doi:10.1111/bpa.12214

Abstract

In Lewy body disease (LBD) such as dementia with LBs and Parkinson's disease, several lines of evidence show that disrupted proteolysis occurs. p62/SQSTM1 (p62) is highly involved with intracellular proteolysis and is a component of ubiquitin-positive inclusions in various neurodegenerative disorders. However, it is not clear whether p62 deficiency affects inclusion formation and abnormal protein accumulation. To answer this question, we used a mouse model of LBD that lacks p62, and found that LB-like inclusions were observed in transgenic mice that overexpressed α-synuclein (Tg mice) with or without the p62 protein. p62 deficiency enhanced α-synuclein pathology with regard to the number of inclusions and staining intensity compared with Tg mice that expressed p62. To further investigate the molecular mechanisms associated with the loss of p62 in Tg mice, we assessed the *mRNA* and protein levels of several molecules, and found that the neighbor of the brca1 gene (*NBr1*), which is functionally and structurally similar to p62, is increased in Tg mice without p62 compared with control Tg mice. These findings suggest that p62 and NBR1 affect the pathogenesis of neurodegenerative diseases through the cooperative modulation of α-synuclein aggregation.

INTRODUCTION

Lewy body disease (LBD) including dementia with LBs and Parkinson's disease (PD) is pathologically characterized by the presence of intracellular inclusions called LBs. α-Synuclein has been identified as a component of LBs (41), and the duplication and triplication of the α-synuclein gene are found in both sporadic and early onset forms of PD (40). Mutations (A30P and A53T) in the α-synuclein gene are linked to autosomal dominant forms of PD (20, 31). Originally, α-synuclein is a proteinase K (PK)-soluble protein that localizes at presynaptic terminals; however, α-synuclein becomes resistant to PK and widely deposited throughout the brain of patients with LBD (19, 42). These findings suggest that α-synuclein is significantly involved in the pathogenesis of both familial and sporadic cases of LBD.

α-Synuclein is physiologically processed by two intracellular degradation systems, including the ubiquitin–proteasome and autophagy–lysosome systems. In case of α-synuclein overload, the autophagy–lysosome system, including chaperone-mediated autophagy, predominantly aids in the degradation of excess α-synuclein (6, 22, 46). Thus, it is possible that dysfunction of intracellular degradation system results in the up-regulation of α-synuclein expression and contributes to abnormal protein accumulation. Indeed, several lysosomal-related genes were identified as a causative mutation in familial PD, including leucine-rich repeat kinase 2 and adenosine-3-phosphate 13A2. Furthermore, PD has been genetically linked to rare lysosomal storage diseases, including Gaucher's disease (25) and Sanfilippo syndrome (47).

p62/SQSTM1/sequestosome 1 (referred to as p62) is a multifunctional protein that is strongly associated with the intracellular degradation system. P62 knockout (KO) mice exhibit mature-onset obesity, insulin and leptin resistance (37). Pathologically, loss of p62 results in the accumulation of hyperphosphorylated tau and insoluble K63-linked polyubiquitin chains (33, 48). p62 contains a ubiquitin-associated (UBA) domain at the C-terminus that enables its interaction with ubiquitinated and misfolded proteins. Additionally, p62 possesses a Phox and Bem1p (PB1) domain at the N-terminus and a LC3 interacting region, suggesting that p62 is able to interact with proteasome components and autophagosomal membranes (29, 38). Thus, it has been suggested that p62 can efficiently degrade ubiquitinated and misfolded proteins through the proteasome and autophagy–lysosome systems. It has been reported that p62 is an inducible protein that easily aggregates under several pathological conditions, such as oxidative

stress and neurodegeneration (1, 11, 27). Accordingly, dysfunction of the intracellular degradation systems induces p62 aggregation *in vivo* (2, 16). Furthermore, loss of p62 suppressed ubiquitin-positive inclusions in neurons of brain-specific autophagy-deficient mice (17). Additionally, ubiquitin- and p62-positive protein aggregates were abrogated in Atg8 and p62 double-mutant flies (26). These findings suggest that p62 may be responsible for the formation of cytoplasmic inclusions and abnormal protein accumulation.

In this study, we used transgenic (Tg) mice overexpressing α-synuclein with a A53T mutation as a model for LBD. We crossed the Tg mice with p62 KO mice to examine the involvement of p62 in abnormal α-synuclein pathology. Immunohistochemical analyses showed that p62 deficiency enhanced α-synuclein pathology, as shown by an increase in inclusion number and staining intensity. We assessed several genes and proteins related to stress response and proteolysis. These data revealed that the expression of neighbor of brca1 gene (NBR1), which is a functional homologue to p62, was increased in p62-deficient mice.

MATERIALS AND METHODS

Animals and experimental design

α-Synuclein Tg mice have been widely used as an animal model for LBD (7, 14, 21, 23, 24, 34, 36, 45). To create this LBD model in a p62-deficient background, we used mice overexpressing human α-synuclein with the A53T mutation under the prion promoter (Jackson Laboratories, Bar Harbor, ME, USA) (7) and p62 KO mice with exon 1–4 deleted as previously described (17). The p62 KO mice lacked abnormal tau pathology. α-Synuclein Tg and p62 KO mice were backcrossed with C57BL/6J mice for at least 10 generations. First, heterozygous α-synuclein Tg mice were bred with p62 KO mice to generate α-synuclein$^{+/-}$/p62$^{+/-}$ mice. Second, α-synuclein$^{+/-}$/p62$^{+/-}$ mice were inbred to generate wild type, p62 KO, α-synuclein$^{+/-}$/p62$^{+/+}$ and α-synuclein$^{+/-}$/p62$^{-/-}$ mice (Figure 1A). Hereafter, wild-type, p62 KO, α-synuclein$^{+/-}$/p62$^{+/+}$ and α-synuclein$^{+/-}$/p62$^{-/-}$ mice are simply referred to as WT, KO, Tg and Tg/KO mice, respectively. All comparisons were made

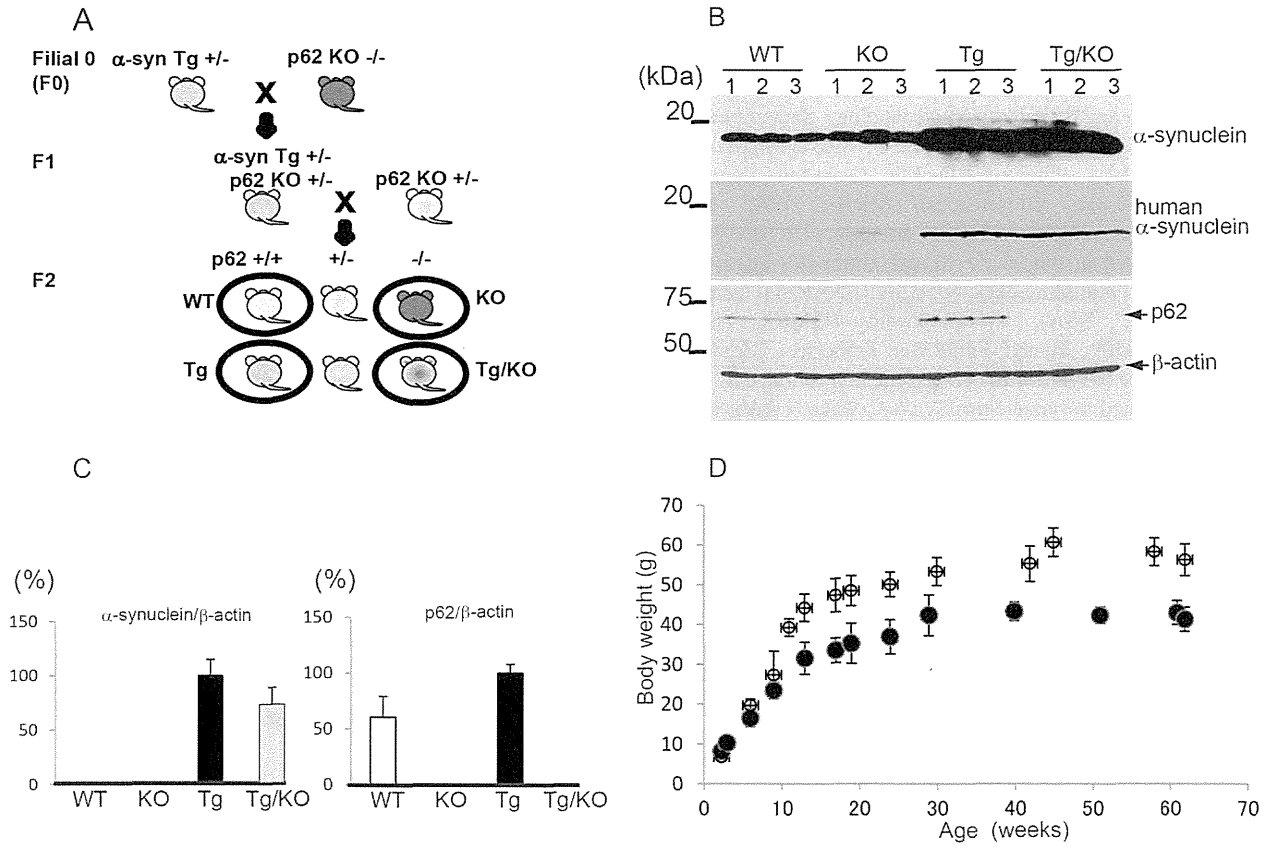

Figure 1. *Characterization of p62 protein deficiency in an animal model of Lewy body disease.* **A.** Breeding strategies to generate p62 deficiency in α-synuclein transgenic (Tg) mice. Initially, heterozygous α-synuclein Tg and homozygous p62-knockout (KO) mice were crossed. Next, littermates and heterozygous p62-deficient mice were mated to generate Tg mice without p62 (Tg/KO), of which four groups were used in this study (black circles). **B.** Immunoblot analysis confirmed that α-synuclein was overexpressed in Tg and Tg/KO mice and that p62 signals were diminished in KO and Tg/KO mice (9 weeks of age, n = 6 per group). The molecular mass is indicated on the left side of the panel. β-Actin was used as a loading control. **C.** A quantitative analysis shows that human α-synuclein is expressed in Tg and Tg/KO mice and that p62 is absent in KO and Tg/KO mice. The values of Tg mice are defined as 100%. **D.** The weight changes of Tg (black circle) and Tg/KO mice (grey circle) are shown (mean ± standard deviation, n = 6–8 per group).

among littermates to minimize confounding effects by different genetic backgrounds. Mice were housed with a light/dark cycle of 12 h and were given food and water *ad libitum*. The experimental protocol was approved by the Institutional Animal Care and Use Committee at the Hirosaki University Graduate School of Medicine in Japan. Tg mice were genotyped using real-time polymerase chain reaction (PCR) analysis (forward primer, 5′-TGT AGG CTC CAA AAC CAA GG-3′; reverse primer, 5′-TAT GCC TGT GGA TCC TGA CA-3′), and verified by backcrossing. Conventional PCR was used for p62 genotyping (primer pair for wild type, forward, 5′-CTT ACG GGT CCT TTT CCC AAC-3′; reverse, 5′-TCC TCC TTG CCC AGA AGA TAG-3′; primer for p62 KO, forward; 5′-CTG CAT GTC TTC TCC CAT GAC-3′; reverse, 5′-TAG ATA CCT AGG TGA GCT CTG-3′). Mice were transcardially perfused with phosphate-buffered saline. The brain was removed, and the right hemisphere was fixed with 4% paraformaldehyde for 48 h. After dehydrating through a graded ethanol series, the right hemisphere was embedded in paraffin and cut into 4-μm thick sections. The left hemisphere was frozen at −80°C for subsequent biochemical analyses.

Antibodies and immunohistochemistry

Rabbit antibodies against Keap1 (ProteinTech Group, Inc., Chicago, IL, USA), p62 (MBL, Nagoya, Japan), NBR1 (Sigma, St. Louis, MO, USA and Santa Cruz Biotechnology, Santa Cruz, CA, USA), NAD(P)H quinone oxidoreductase 1 (NQO1) (Sigma), LC3 (Sigma and MBL), ubiquitin (DAKO, Glostrup, Denmark), UBQLN1 (Lifespan Biosciences, Seattle, WA, USA), phosphorylated α-synuclein (Abcam, Cambridge, UK) and β-actin (Sigma) were used in this study. Mouse antibodies against p62 (BD Biosciences, Franklin Lakes, NJ, USA), SNAP25 (Chemicon, Temecula, CA, USA), synaptophysin (DAKO), human α-synuclein (LB509; Zymed, South San Francisco, CA, USA), human and mouse α-synucleins (4D6; GeneTex, Irvine, CA, USA) and phosphorylated α-synuclein (pSyn#64; Wako, Osaka, Japan) were also used.

The sections were dehydrated and pretreated with heat retrieval using an autoclave for 10 minutes in 10 mM citrate buffer (pH 6.0) for rabbit anti-Keap1 and anti-NBR1 antibodies. The sections were then subjected to immunohistochemical processing using the avidin-biotin-peroxidase complex method with diaminobenzidine (Sigma). In addition, the sections were counterstained with hematoxylin. For the staining of presynaptic PK-resistant α-synuclein, sections were pretreated with PK (Gibco BRL, Gaithersburg, MD, USA; 50 μg/mL) in a PK buffer containing 10 mM Tris-HCl, pH 7.8, 100 mM NaCl, 0.1% Nonidet-P40 at 37°C for 5 minutes. The total number of inclusions immunostained with anti-phosphorylated α-synuclein was quantified in contiguous sections. Immunohistochemical studies were performed at 9 weeks of age (n = 6 per group).

Quantitative reverse transcription-polymerase chain reaction (qRT-PCR)

Total RNA was extracted from the right hemisphere of the brain using the RNeasy lipid tissue mini kit (Qiagen, Hilden, Germany) at 9 weeks of age (n = 3 per group). cDNA was synthesized from 1 μg of total RNA using the PrimeScript® II first-strand cDNA synthesis kit (Takara Bio Inc., Otsu, Japan). An aliquot of cDNA was used for gene expression analysis with the SYBR® Premix Ex Taq™ II (Perfect Real Time) (Takara Bio Inc.) and CFX Real-Time PCR Detection System (Bio-Rad, Hercules, CA, USA) using the following primer sets: heme oxygenase-1 (*Ho-1*) (5′-CCA GCA ACA AAG TGC AAG ATT C-3′; 5′-TCA CAT GGC ATA AAG CCC TAC AG-3′), *Nqo1* (5′-GTC ATT CTC TGG CCA ATT CAG AGT-3′; 5′-TTC CAG GAT TTG AAT TCG GG-3′), glutamate-cysteine ligase catalytic subunit (*Gclc*) (5′-AAA ATG CGG AGG CAT CAA-3′; 5′-ATA TGC TGC AGG CTT GGA AT-3′), *p62* (5′-AGC TGC CTT GTA CCC ACA TC-3′; 5′-CAG AGA AGC CCA TGG ACA G-3′), *Cyclophilin A* (5-ATG CTG GAC CCA ACA CAA AT-3′; 5-TCT TTC ACT TTG CCA AAC ACC-3′), *Keap1* (5′-CAC AGC AGC GTG GAG AGA-3′; 5′-CAA CAT TGG CGC GAC TAG A-3′), *Lamp1* (5′-CCT ACG AGA CTG CGA ATG GT-3′; 5′-CCA CAA GAA CTG CCA TTT TTC-3′), *Cathepsin D* (5′-CCC TCC ATT CAT TGC AAG ATA C-3′; 5′-TGC TGG ACT TGT CAC TGT TGT-3′), *transcription factor EB* (*TfEB*) (5′-GAG CTG GGA ATG CTG ATC C-3′; 5′-GGG ACT TCT GCA GGT CCT T-3′); *Rab7l1* (5′-GCT GCA GCA CTG GGA TAT TG-3′; 5′-TAG TAG AGT CGT GTC ATG GAT GTG-3′) and *Nbr1* (5′-TCA ACA GGA CTC GCA AAC AG-3′; 5′-ATG CTG CTC CCA TTG TGG-3′). *Cyclophilin A* was used for normalization.

Immunoblot analysis

Western blot analysis was performed as previously described (43). For total cell lysate, we used a lysis buffer with 4% sodium dodecyl sulfate (SDS; 75 mM Tris-HCl, pH 6.8, 4% SDS, 25% glycerol, 5% β-mercaptoethanol) and passed sample through 21 gauge needle attached on a 1 mL syringe. For an experiment using insoluble sample of detergent, samples were weighted and lysed with 10-fold volume of Tris-based buffer (pH 7.4) containing 0.1% Triton X-100 on ice. After homogenization with a pestle 20 times, they were passed 10 times through 21 gauge needle attached on a 1 mL syringe. Lysates were incubated for 5 minutes on ice, and centrifuged at 12 000 × g for 10 minutes. Supernatant was used as a soluble fraction. The pellets were resuspended with 8 M urea and sonicated (insoluble fraction). Signal detection was performed according to the protocol provided with the ECL or ECL prime detection systems (Amersham Pharmacia Biotech, Piscataway, NJ, USA). We performed each immunoblot analysis a minimum of three times, and all data were quantified and collected.

Animal behavioral testing

The Morris water maze

Spatial learning was assessed in a round tank of water (0.95 m in diameter) at 30°C. An escape platform (10 cm in diameter) was placed 1 cm below the water surface. A camera (Primetech Engineering Corp., Tokyo, Japan) was mounted above the maze and attached to a computer running the Smart software (Primetech Engineering Corp.). The training paradigm for the hidden platform version of the Morris water maze consisted of two trials per day for five consecutive days. The time taken to reach the platform (latency to escape) was recorded for each trial. The time limit was 120 s, and the intertrial interval was 1 h. If the animal could not

find the platform, it was placed on the platform for 20 s. After removing the platform, the probe trial was carried out 2 h after the completion of training on the fifth day. The latency to reach the former location of the platform and the percentage of total time spent in each quadrant were recorded.

Forced swim test

Immobility time was analyzed using a forced swim test. Animals were individually placed in a transparent acrylic cylindrical beaker (height: 25 cm, diameter: 18 cm) containing 4600 mL of clear water at 25 ± 1°C for 6 minutes. A mouse was judged to be immobile when it remained passively floating in the water for more than 2 s. Immobility time was quantified using a Forced Swim Scan software (Clever Sys Inc., Reston, VA, USA).

Quantitative analysis and statistical analysis

A semi-quantitative analysis of protein levels was performed using the ImageJ software provided by the NIH. All data were represented as the mean + standard deviation. The statistical significance was evaluated using one-way analysis of variance (ANOVA) with Bonferroni's post hoc test to analyze four genotypes and Student's *t*-test to analyze two genotypes. A probability value of less than 0.05 ($P < 0.05$) was considered to be significant.

RESULTS

Characterization of α-synuclein Tg mice with or without p62

To test the possibility that p62 is responsible for the formation of cytoplasmic inclusions and abnormal protein accumulation, we generated mice that overexpressed human α-synuclein (Tg) on a p62-deficient background (Figure 1A). First, we crossed Tg mice with p62 KO mice. Next, littermates with or without p62 and/or human α-synuclein were selected by genotyping and crossed to generate Tg mice lacking p62. Consequently, littermates with or without endogenous p62 and/or human α-synuclein expression were born at the expected Mendelian ratio. For our studies, we used WT, KO, Tg and Tg/KO mice.

We confirmed that α-synuclein was robustly expressed in the brains of Tg mice and Tg/KO mice (Figure 1B). We used a human α-synuclein-specific antibody, LB509, to confirm that human α-synuclein expression was present only in Tg and Tg/KO mice. There were no differences in the endogenous and human α-synuclein levels between the Tg and Tg/KO mice. We also confirmed that p62 protein levels were diminished in the brains of KO and Tg/KO mice. Interestingly, the amount of p62 was slightly higher in Tg mice than it was in WT mice (Figure 1C). An increase of p62 was also supported by immunohistochemical studies that showed an increase in p62 immunoreactivity in Tg mice compared with WT mice (Figure 2A). α-Synuclein expression was mainly observed in the presynapses in the brains of WT and p62 KO mice; however, additional staining of α-synuclein was observed in the cytoplasm and presynapses in the brains of Tg and Tg/KO mice (Figure 2B). Consistent with previous papers (28, 37), KO mice exhibited mature-onset obesity. As they aged, Tg/KO mice had a heavier average body weight than did Tg mice (Figure 1D). The majority of Tg mice remained healthy until at least 70 weeks of age. Tg and Tg/KO mice were behaviorally indistinguishable and displayed lower food intake and activity at the end stage of the disease.

Tg/KO mice exhibit an increase in phosphorylated α-synuclein staining and inclusion number compared with Tg mice

Similar to the human pathological conditions, there are two types of abnormal α-synuclein in the brains of Tg mice (7, 42), including phosphorylated α-synuclein (P-syn) and PK-resistant α-synuclein (PK-syn). Immunohistochemical analyses showed that P-syn is observed in both Tg/KO and Tg mice (Figure 3A). We compared the number of P-syn-positive inclusions in the thalamus of Tg and Tg/KO mice. Quantitative data indicated that the number of inclusions was higher in Tg/KO mice compared with Tg mice (Figure 3B). Furthermore, the intensity of P-syn staining was increased in the hippocampus and cerebral cortex of Tg/KO mice compared with Tg mice (Figure 3C). Unlike human pathological conditions, p62 was not localized in the cytoplasmic inclusions in the brains of Tg mice. Immunohistochemical studies demonstrated that PK treatment abolished normal α-synuclein immunoreactivity, and PK-syn was found in the presynapses of the brain of both Tg and Tg/KO mice (Figure 3D). Western blot analysis verified that P-syn signal intensity was higher in Tg/KO than Tg mice using two kinds of antibodies against P-syn (Figure 3E). Furthermore, we fractionated samples of Tg and Tg/KO mice by buffer with 0.1% Triton X-100 detergent, and found that insoluble P-syn level was increased in Tg/KO compared with Tg mice (Figure 3F). Thus, p62 deficiency modulates α-synuclein pathology with regard to P-syn staining intensity, the number of P-syn inclusions and solubility.

Behavioral tests revealed a longer immobility time for p62-deficient mice

Given the presynaptic aggregation of PK-syn in the hippocampus of Tg and Tg/KO mice, we sought to determine whether memory function was also affected in these mice. We performed the Morris water maze test using mice at a younger age (9 weeks old) to exclude differences in body weight. The average weight was comparable between Tg and Tg/KO mice (21.1 g in Tg, 22.0 g in Tg/KO) at 9 weeks of age. During the training phase of the Morris water maze test, WT and Tg mice showed a gradual decrease in escape latency over time; however, KO and Tg/KO mice exhibited longer escape latencies (Supporting Information Video Clip S1 and S2). When the platform was removed, 80% of WT mice and 70% of Tg mice found the platform location. In contrast, less than 50% of KO and Tg/KO mice found the platform location. KO and Tg/KO mice took a longer time to reach to the platform location (Figure 4A) and spent less time in the target quadrant (Figure 4B) than did WT mice. The lower rate of platform crossing in the KO mice was due to their immobility (Figure 4C,D), which is consistent with previous results showing that KO mice exhibited immobility during training and probe trials (33). During only the first minute of a forced swim test, KO mice showed a significantly increased immobility that lasted longer than 2 s when compared with WT mice (Figure 4E,F). Thereafter, the time course for

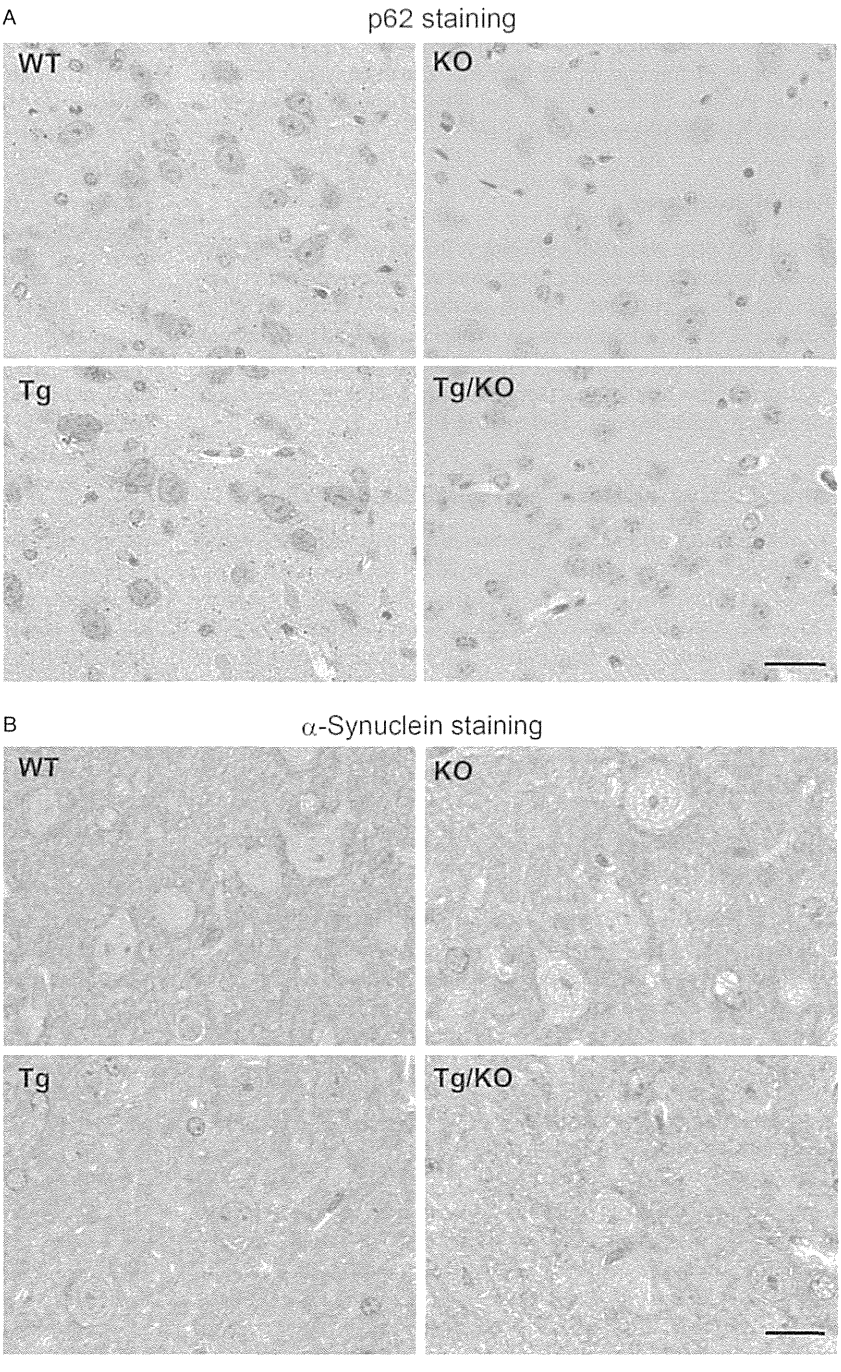

Figure 2. *p62 and α-synuclein staining in wild-type (WT), knockout (KO), Tg and Tg/KO mice.* **A.** Immunohistochemical analysis shows that p62 immunoreactivity is observed in WT and Tg mice but not in KO mice (9 weeks of age, n = 6 per group). Bar = 20 μm. **B.** Human and mouse α-synuclein is strongly expressed in the presynapse and cytoplasm of cortical neurons in Tg and Tg/KO mice. Bar = 10 μm.

floating behavior (the percentage of immobility) was similar between groups. There was no significant difference between Tg/KO and WT mice. These results suggest that p62 plays a role in maintaining neurological functions, such as stress responses and motivation to escape.

Increased levels of the functional homologue, NBR1, in p62 KO and Tg/KO mice

To analyze the molecular mechanisms associated with the loss of p62 on Tg mice, we performed quantitative RT-PCR analysis using primers for genes related to the stress response and proteolysis (Figure 5). Consistent with the genotype results, the *p62 mRNA* level was diminished in KO and Tg/KO mice. Keap1 is a binding partner of p62 and functions as a sensor for noxious stimuli such as oxidants and electrophiles. The *mRNA* level of *Keap1* appeared to be different between the four groups; however, the data were not statistically significant ($P = 0.069$). Previous papers have reported that autophagy-deficient mice display a higher expression of detoxifying enzymes, such as *Ho-1*, *Nqo1* and *Gclc* (18). There were no differences in the *mRNA* levels of these enzymes among the four groups. Recent evidence indicates that α-synuclein

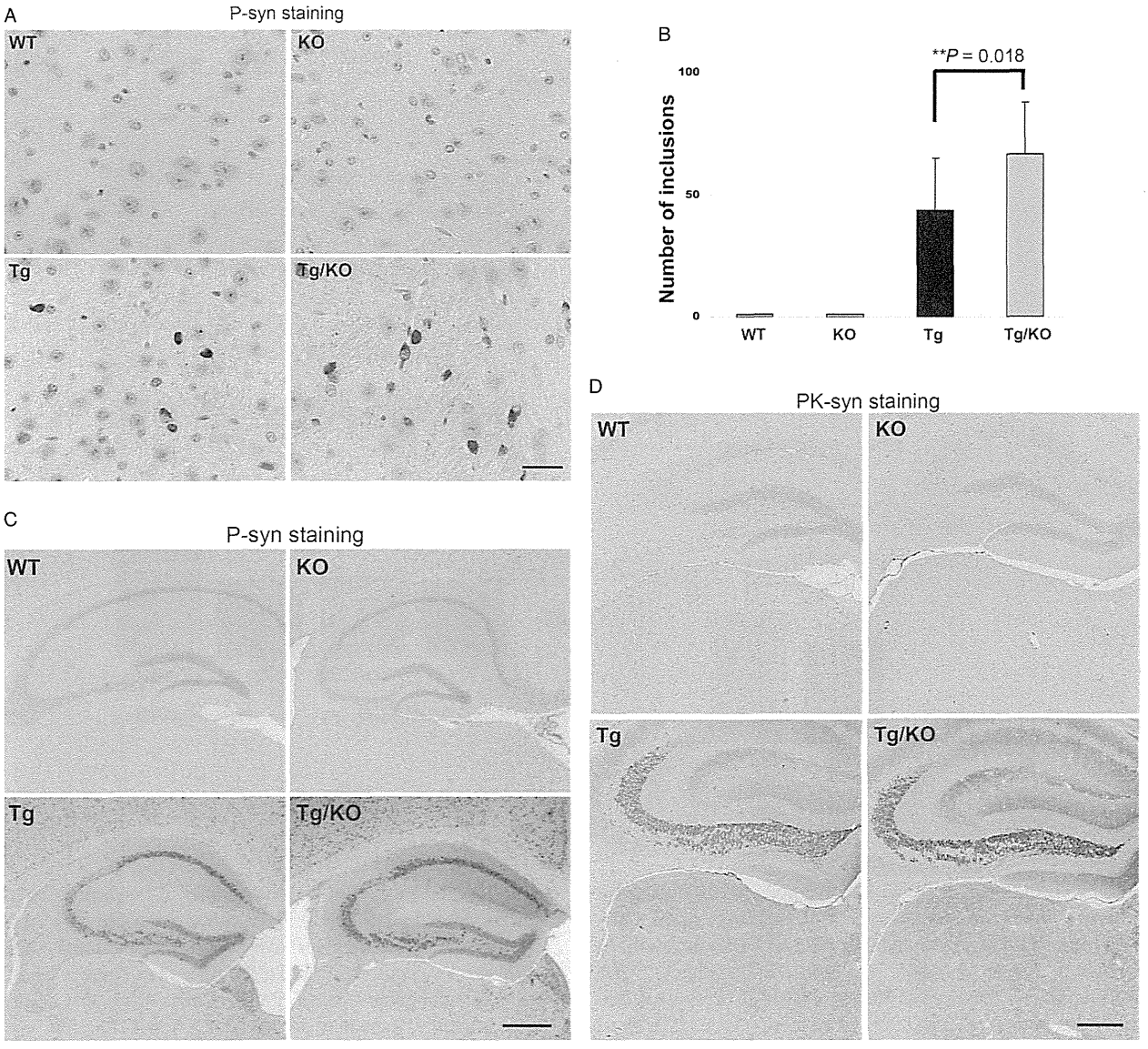

Figure 3. *The effect of p62 deficiency on abnormal α-synuclein expression.* **A.** Cytoplasmic inclusions are positive for phosphorylated α-synuclein (P-syn) in the thalamus of Tg and Tg/knockout (KO) mice. Bar = 20 μm. **B.** A quantitative analysis shows that the number of cytoplasmic inclusions is significantly increased in Tg/KO mice when compared with Tg mice (9 weeks of age, n = 6 per group). The groups differed significantly [analysis of variance (ANOVA), $F(3, 11) = 160.81$, $P < 0.01$]. **C.** P-syn staining is observed in the neurons of the cerebral cortex and hippocampus in Tg and Tg/KO mice. An increased staining intensity is observed in Tg/KO mice compared with Tg mice. Bar = 500 μm. **D.** No obvious differences in proteinase K-resistant α-synuclein (PK-syn) are found between Tg and Tg/KO mice. Bar = 250 μm. **E.** P-syn level is significantly increased in Tg/KO mice compared with Tg mice. Ratio of P-syn to β-actin was calculated, and the values of Tg mice are defined as 1.0. The groups differed significantly [ANOVA, $F(3, 11) = 147.1$, $P < 0.01$]. **F.** Triton X-100 soluble and insoluble samples were prepared from Tg and Tg/KO mice (9 weeks of age, n = 2 per Tg and Tg/KO groups). Insoluble P-syn level is increased in Tg/KO mice compared with Tg mice. P-syn levels were normalized by total synuclein, and the values of Tg mice were defined as 1.0 in a soluble or insoluble sample.

overexpression causes dynamic changes in the autophagy–lysosomal system. Therefore, we assessed levels of *TfEB*, a major transcriptional regulator for this system (39), lysosomal enzymes (*Lamp1* and *cathepsin D*), molecules responsible for membrane trafficking (*Rab7l1*) and selective autophagy markers (*Nbr1*). Among these genes, only the *Nbr1 mRNA* levels were significantly different ($P < 0.01$) between the four groups. Consistent with this result, the NBR1 protein levels were significantly increased in mice lacking p62 compared with mice with p62 ($P < 0.05$) (Figure 6A,B). Additionally, Keap1 protein levels were also significantly different among the four groups at the protein level. There were no alterations in NQO1, synaptic proteins and proteolysis-related molecules, such as ubiquitin and LC3, which are essential to autophagosomal formation (13). Based on the

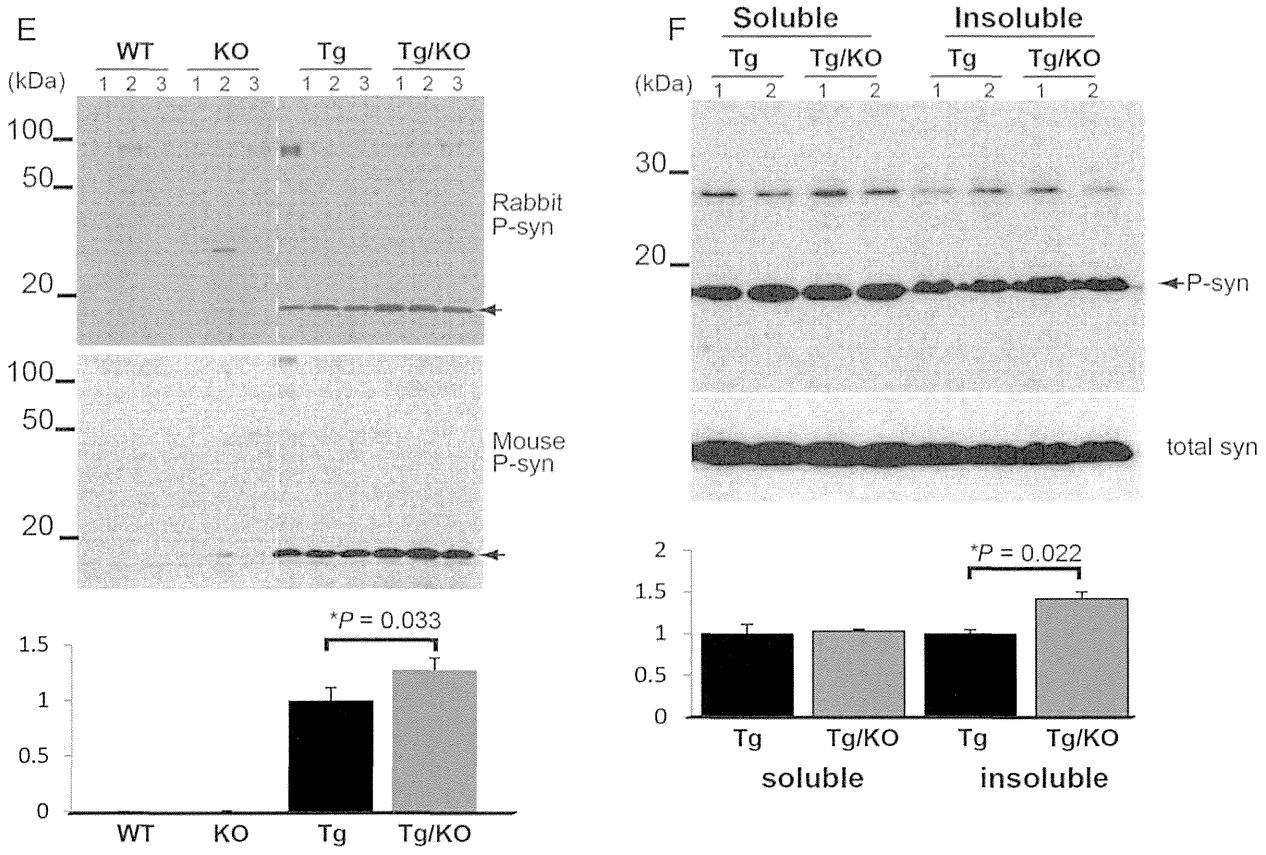

Figure 3. *Continued.*

increased NBR1 levels in mice lacking p62, we compared the distribution patterns of p62 and NBR1 in the mouse brain. Interestingly, immunoblotting showed that p62 and NBR1 are similarly distributed in distinct regions of the mouse brain (Figure 7A,B). NBR1 was mainly localized in the cytoplasm of neurons, and its intensity was higher in Tg/KO than in Tg mice (Figure 7C). These data are consistent with the qRT-PCR and immunoblotting analyses.

DISCUSSION

p62 is an inducible protein that easily aggregates under pathological conditions, such as oxidative stress and disrupted proteolysis, and it is localized in cytoplasmic inclusions in LBD and other neurodegenerative diseases, suggesting that p62 contributes to inclusion formation. Moreover, p62- and ubiquitin-positive inclusions in the neurons of brain-specific *Atg7*-deficient mice disappear with the loss of p62 (17). Based on these findings, we initially predicted that p62 deficiency would lead to a decrease in the number of inclusions in Tg mice that overexpressed α-synuclein. However, our data suggest that p62 deficiency results in an exaggeration of α-synuclein pathology with regard to P-syn staining intensity and inclusion number. Consistent with our findings, Doi *et al* demonstrated that a loss of p62 exacerbated neuropathological outcomes (5) in a mouse model of spinal and bulbar muscular atrophy, which is one of polyglutamine diseases. Our pathological data showed that the number of P-syn-positive inclusion increased by 1.5-fold in Tg/KO mice compared with Tg mice. Consistently, this was supported by Western blot analyses showing that P-syn level was higher in Tg/KO mice than Tg mice using two kinds of antibodies against P-syn. Considering that increased P-syn is mainly resistant to detergent of Triton X-100, it is possible that biochemical property of α-synuclein is altered and leads to more aggregation in Tg/KO mice. Although it remains controversial whether the formation of cytoplasmic inclusions exerts a beneficial or toxic effect on cells, our findings strengthen the idea that p62 can modulate α-synuclein aggregation and the pathogenesis of diseases.

Consistent with previous results (28, 37), a p62 deficiency resulted in mature-onset obesity in mice. Recent evidence indicates that hyperphagia is the primary cause of obesity in p62-deficient mice due to the disruption of leptin signaling (9). Accordingly, p62 is highly expressed in hypothalamic neurons, including proopiomelanocortin (POMC) neurons in the arcuate nucleus (3, 9) that are responsible for the control of appetite and energy intake. Interestingly, lack of autophagic activity in POMC neurons caused higher post-weaning body weight and p62/ubiquitin aggregation (4, 32). Furthermore, leptin signaling is also disrupted in these mice. This may have broad implications for the pathophysiology of p62 KO mice. Because p62 helps shuttle insoluble and ubiquitinated proteins into autophagosomes, disruption of autophagic flux or loss of p62 gives rise to the accumulation

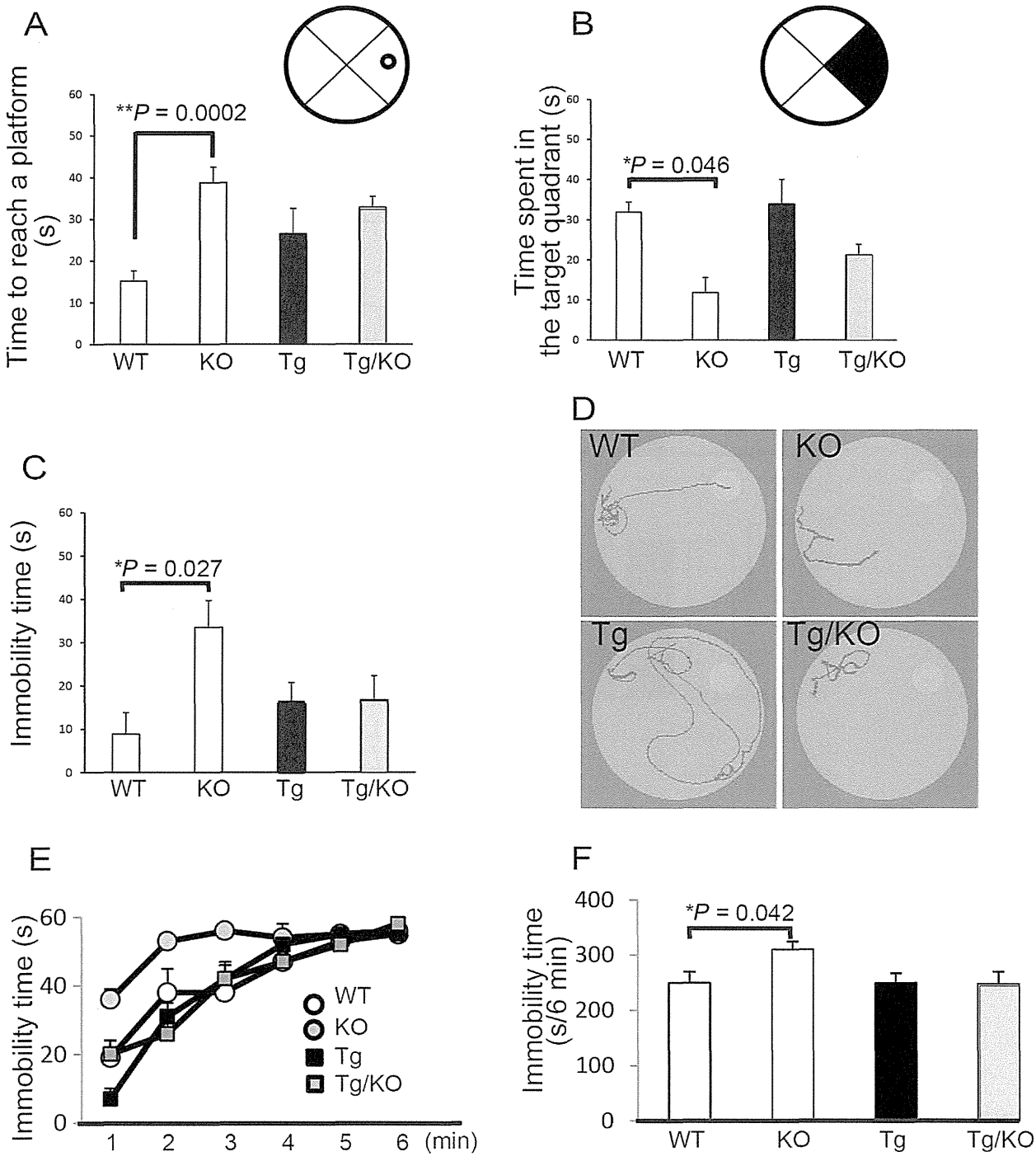

Figure 4. *p62-deficient mice exhibit longer escape latencies due to lower activity.* **A.** The probe trial was completed after 5 days of hidden platform training in the Morris water maze. Wild type (WT, n = 10), p62 knockout (KO, n = 11), α-synuclein Tg (Tg, n = 9) and α-synuclein mice lacking p62 (Tg/KO, n = 9) were tested at 9 weeks of age. KO mice take longer to reach the platform location. The groups differed significantly [analysis of variance (ANOVA), $F(3, 39) = 4.53$, $P < 0.01$]. **B.** The percentage of time spent in the target quadrant (black) during a 60 s probe trial of the Morris water maze test. KO mice spend less time in the target quadrant. **C.** The immobility time of the Morris water maze. Longer immobility times are evident in KO mice. **D.** Representative path tracings are shown. Light pink indicates the position of the platform. **E.** A forced swim test was performed at 9–10 weeks of age (n = 9–11 per group) and shows a significant difference in immobility latency, with KO mice lasting longer than 2 s and WT mice remaining mobile for the first 1 minute. **F.** KO mice exhibit higher immobility times for the first 6 minutes. The groups differed significantly [ANOVA, $F(3, 39) = 2.14$, $P < 0.05$]. $^*P < 0.05$.

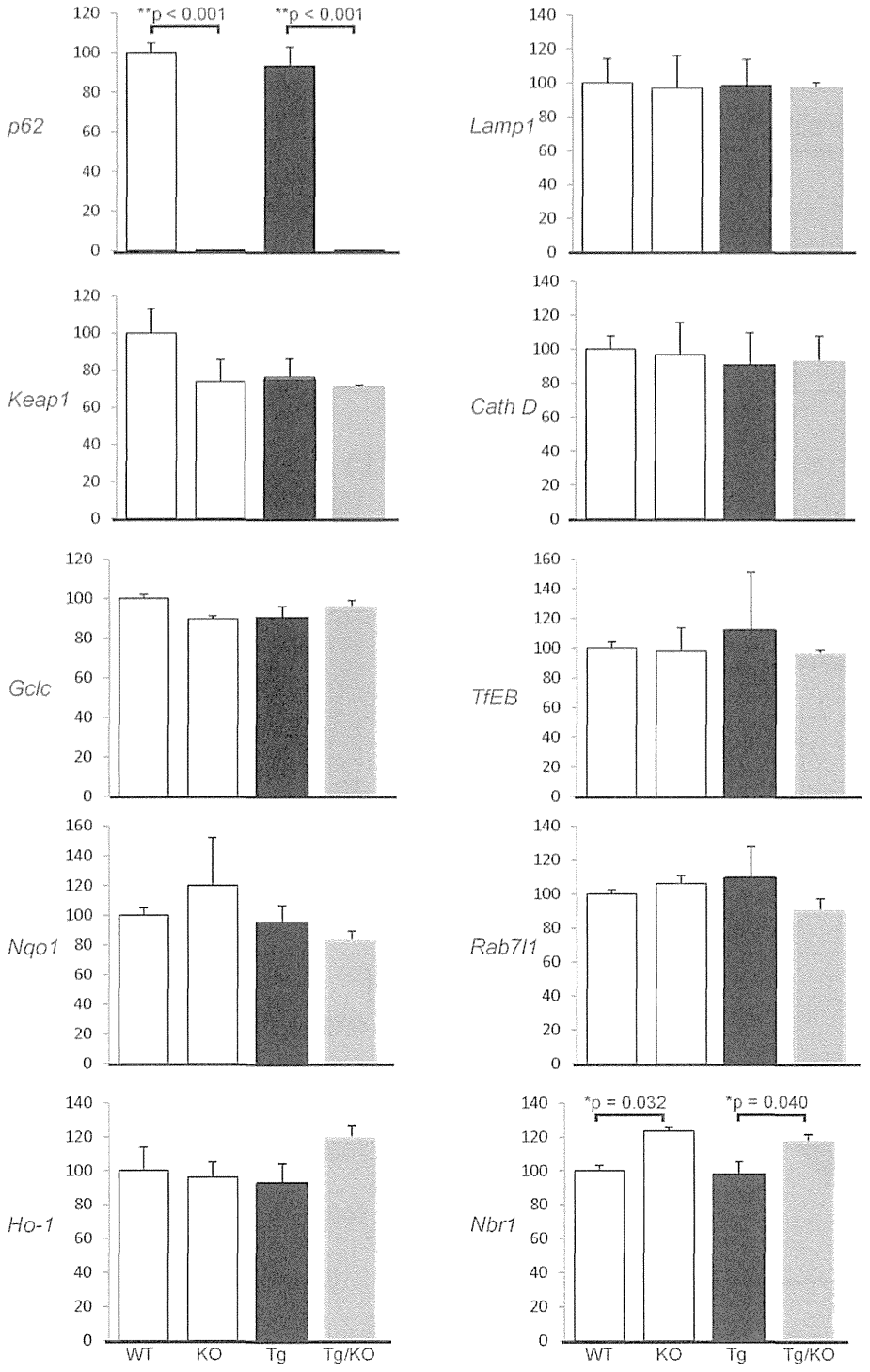

Figure 5. *The effect of p62 deficiency on several kinds of genes.* The *mRNA* levels of genes related to proteolysis and oxidative stress in the brains of WT, KO, Tg and TG/KO mice were determined at 9 weeks of age (n = 3 per group). *mRNA* was measured by quantitative reverse transcription-polymerase chain reaction (qRT-PCR) using the right hemisphere of the brain. Data are normalized by the *Cyclophilin A mRNA* level in each sample, and the average and standard deviation was calculated. qRT-PCR reveals that there is no significant difference in the *Keap1*, glutamate-cysteine ligase catalytic subunit (*Gclc*), NAD(P)H quinone oxidoreductase 1 (*Nqo1*), heme oxygenase-1 (*Ho-1*), *Lamp1*, *Cathepsin D*, *TfEB* and *Rab7l1* levels among the four groups. In contrast, the *mRNA* level of *p62* ($P < 0.01$) and *Nbr1* ($P < 0.05$) are significantly different. The groups differed significantly [analysis of variance, $F(3, 11) = 226.86$, $P < 0.01$ in *p62 mRNA*, $F(3, 11) = 14.15$, $P < 0.01$ in *Nbr1 mRNA*]. The WT values are defined as 100%. $*P < 0.05$, $**P < 0.01$.

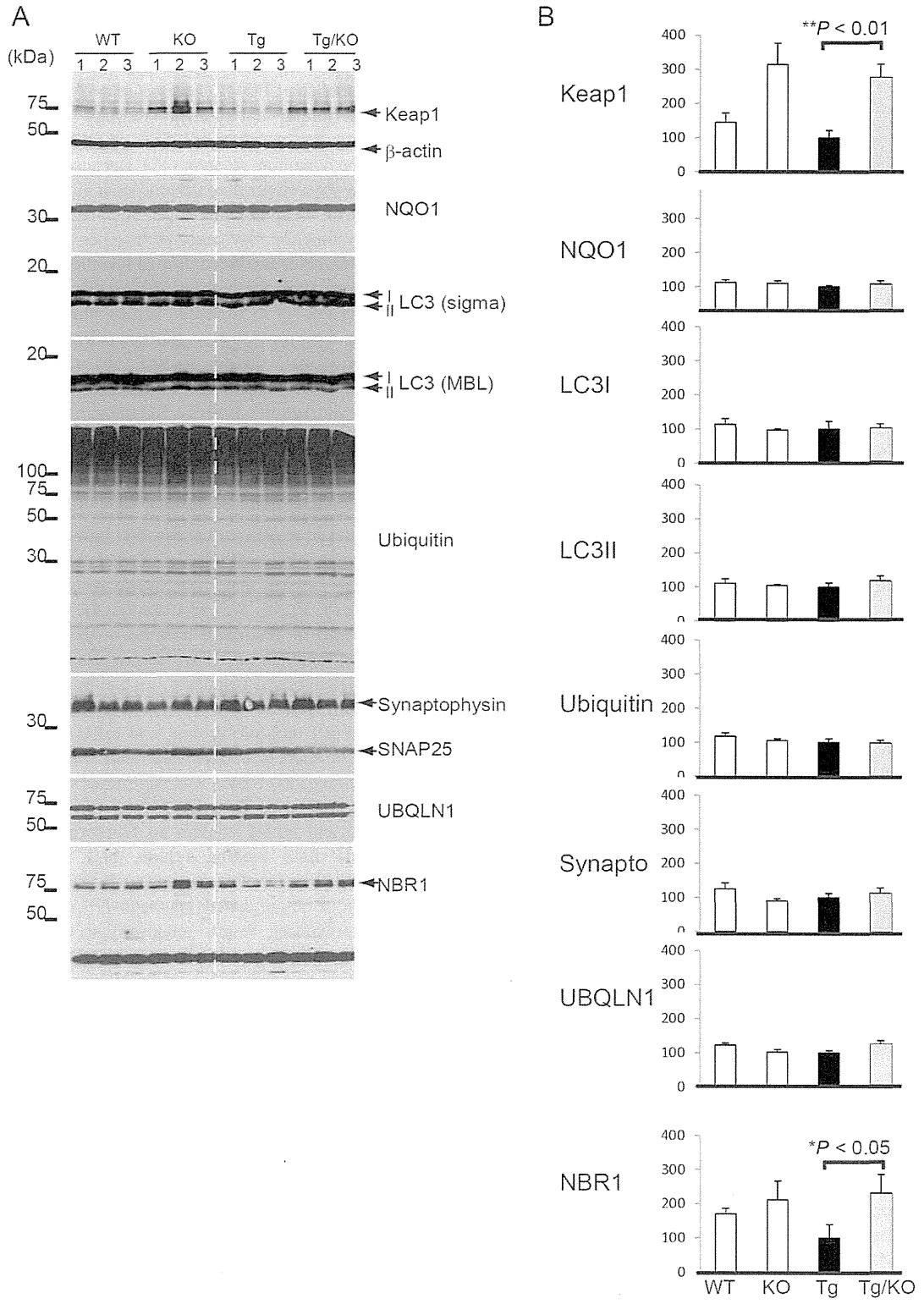

Figure 6. *The effect of p62 deficiency on molecules related to proteolysis, oxidative stress and the synapse.* **A.** Expression of Keap1 and NBR1 is significantly increased in Tg/KO mice compared with Tg mice. NAD(P)H quinone oxidoreductase 1 (NQO1), LC3, ubiquitin, synaptophysin and SNAP25 levels are not significantly different between the four groups (9 weeks of age, n = 6 per group). **B.** A quantitative analysis indicates that the Keap1 and NBR1 levels are significantly increased in p62-deficient mice compared with mice with p62. The Tg values are defined as 100%. $*P < 0.05$, $**P < 0.01$. The groups differed significantly [analysis of variance, $F(3, 11) = 7.44$, $P = 0.011$ in Keap1, $F(3, 11) = 4.27$, $P = 0.045$ in NBR1].

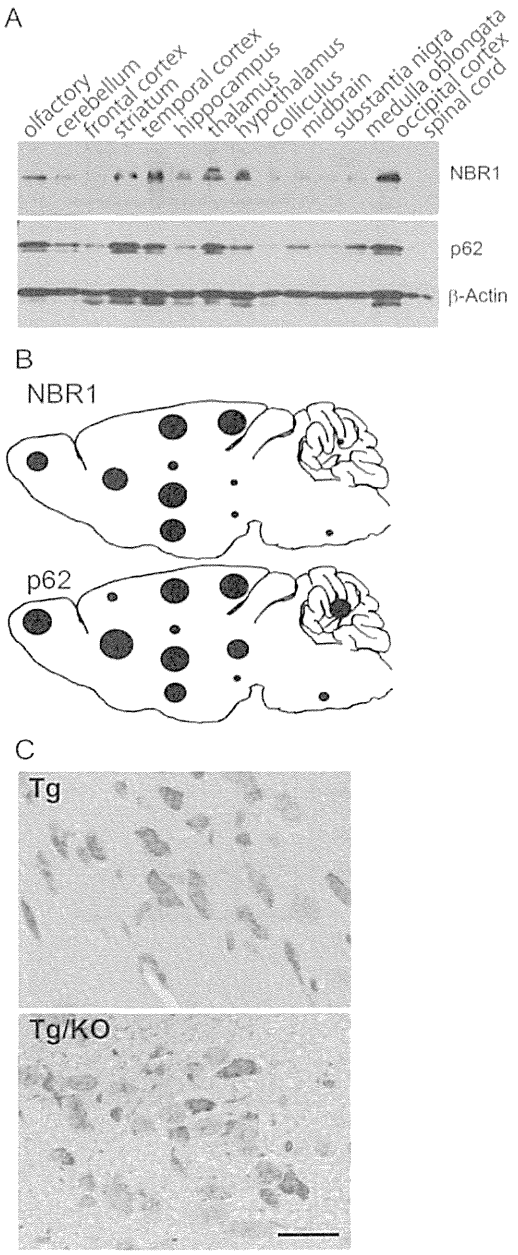

Figure 7. *The spatial patterns of p62 and NBR1 in the mouse brain.* **A.** Equal amounts of homogenates from the indicated regions were analyzed by immunoblotting (12 weeks of age, n = 2 in wild-type mice). Antibodies against NBR1 (upper) or p62 (bottom) were used to detect endogenous proteins. NBR1 is mainly expressed in the olfactory bulb, temporal and occipital cortices, striatum, thalamus and hypothalamus. The highest expression of p62 is observed in the olfactory bulb, striatum, temporal and occipital cortices, hippocampus, thalamus, hypothalamus and medulla oblongata. β-Actin is used as a loading control. **B.** Distribution patterns of NBR1 and p62 in the sagittal section of mice brains. NBR1 or p62 levels are normalized by β-actin. The circles represent the size of the expression level. **C.** NBR1 immunostaining in Tg and Tg/KO mice (9 weeks of age, n = 6 per group). NBR1 immunoreactivity is mainly detected in neurons of the thalamus of both Tg and Tg/KO mice. Note the increased intensity of NBR1 immunoreactivity in Tg/KO mice compared with Tg mice. Bar = 30 μm.

of p62 target molecules. Accordingly, we revealed that P-syn level is increased in Triton X-100 insoluble fraction of Tg/KO mice compared with Tg mice. Thus, p62 dysfunction observed in autophagy-deficient POMC neurons or p62 KO mice might also affect intercellular environment through disturbance of p62 binding partners or substrates. One of p62 binding partners is known to be dopamine receptor (15). Because dopamine is widely involved in physiological conditions such as mood, cognition and motor control, it is possible that p62 modulates dopamine system, and p62 dysfunction may cause pathogenesis of PD.

Our immunoblot results confirmed that the hypothalamus is one of the regions with the highest p62 expression level. The hypothalamus is known to regulate various physiological functions, particularly the hypothalamus-pituitary-adrenal axis, which coordinates emotional, neuroendocrine and autonomic inputs in response to stress. Regarding behavioral abnormalities, we could not distinguish Tg mice from Tg/KO mice; however, p62-deficient mice exhibited less activity and depression-like behavior in the Morris water maze and forced swim test. This is consistent with previous results (33). It is conceivable that p62 deficiency affects the hypothalamus-pituitary-adrenal axis, leading to behavioral abnormalities in response to stress. The immobility rate of Tg/KO mice was comparable with that of normal control mice. Considering previous reports that mice overexpressing α-synuclein are hyperactive (8, 30, 44), we speculate that the degree of immobility in Tg/KO mice is recovered because of the hyperactivity of Tg mice. Taken together, p62 plays an important role in modulating multiple physiological responses, including nutritional, oxidative and water stressors.

We screened multiple protein and *mRNA* levels to study the molecular mechanisms associated with the loss of p62 in Tg mice. We found that NBR1 was significantly increased in Tg/KO mice compared with Tg mice at both the *mRNA* and protein levels. p62 and NBR1 contain an N-terminal PB1 domain, an intermediate LC3 binding region, and a C-terminal UBA domain, and they function as cargo adapters for the autophagic degradation of ubiquitinated substrates (10, 12, 29). Intriguingly, our immunoblotting results suggest that these molecules are similarly distributed in distinct regions of the mouse brain. This spatial pattern and functional similarity raise the possibility that NBR1 levels can be up-regulated to compensate for the loss of p62 protein. Therefore, the functional redundancy of NBR1 may mask the anticipated abnormalities of p62-deficient mice.

In conclusion, we have provided evidence that p62 is unnecessary for the formation of inclusions in an animal model that overexpresses α-synuclein. In addition, p62 deficiency enhanced α-synuclein pathology based on the number of inclusions and staining intensity of P-syn. In support of this finding, it is likely that p62 indirectly helps sequester abnormal molecules through its own oligomerization (35). Further analyses at the molecular level suggest that NBR1 plays a compensatory role for p62 in the central nervous system. NBR1 and p62 double KO mice would be a useful tool to test this hypothesis.

ACKNOWLEDGMENTS

This work was supported by JSPS KAKENHI grant numbers 26430050 (K.T.), 26860655 (Y.M.), 26430049 (F.M.), 24300131

(K.W.); Priority Research Grant for Young Scientists designated by the president of Hirosaki University (K.T., J.M.); Hirosaki University Institutional Research Grant (K.I., K.W.); grants-in-aid from the Research Committee for Ataxic Disease from the Ministry of Health, Labor and Welfare, Japan (K.W.); and an Intramural Research Grant (24-5) for Neurological and Psychiatric Disorders of NCNP (K.W.). The authors wish to express their gratitude to K. Saruta, T. Kon, M. Nakata and A. Ono for their technical assistance.

REFERENCES

1. Bartlett BJ, Isakson P, Lewerenz J, Sanchez H, Kotzebue RW, Cumming RC *et al* (2011) p62, Ref(2)P and ubiquitinated proteins are conserved markers of neuronal aging, aggregate formation and progressive autophagic defects. *Autophagy* **7**:572–583.
2. Bedford L, Hay D, Devoy A, Paine S, Powe DG, Seth R *et al* (2008) Depletion of 26S proteasomes in mouse brain neurons causes neurodegeneration and Lewy-like inclusions resembling human pale bodies. *J Neurosci* **28**:8189–8198.
3. Braak H, Thal DR, Del Tredici K (2011) Nerve cells immunoreactive for p62 in select hypothalamic and brainstem nuclei of controls and Parkinson's disease cases. *J Neural Transm* **118**:809–819.
4. Coupe B, Ishii Y, Dietrich MO, Komatsu M, Horvath TL, Bouret SG (2012) Loss of autophagy in pro-opiomelanocortin neurons perturbs axon growth and causes metabolic dysregulation. *Cell Metab* **15**:247–255.
5. Doi H, Adachi H, Katsuno M, Minamiyama M, Matsumoto S, Kondo N *et al* (2013) p62/SQSTM1 differentially removes the toxic mutant androgen receptor via autophagy and inclusion formation in a spinal and bulbar muscular atrophy mouse model. *J Neurosci* **33**:7710–7727.
6. Ebrahimi-Fakhari D, Cantuti-Castelvetri I, Fan Z, Rockenstein E, Masliah E, Hyman BT *et al* (2011) Distinct roles in vivo for the ubiquitin-proteasome system and the autophagy-lysosomal pathway in the degradation of alpha-synuclein. *J Neurosci* **31**:14508–14520.
7. Giasson BI, Duda JE, Quinn SM, Zhang B, Trojanowski JQ, Lee VM (2002) Neuronal alpha-synucleinopathy with severe movement disorder in mice expressing A53T human alpha-synuclein. *Neuron* **34**:521–533.
8. Graham DR, Sidhu A (2010) Mice expressing the A53T mutant form of human alpha-synuclein exhibit hyperactivity and reduced anxiety-like behavior. *J Neurosci Res* **88**:1777–1783.
9. Harada H, Warabi E, Matsuki T, Yanagawa T, Okada K, Uwayama J *et al* (2013) Deficiency of p62/Sequestosome 1 causes hyperphagia due to leptin resistance in the brain. *J Neurosci* **33**:14767–14777.
10. Ichimura Y, Kumanomidou T, Sou YS, Mizushima T, Ezaki J, Ueno T *et al* (2008) Structural basis for sorting mechanism of p62 in selective autophagy. *J Biol Chem* **283**:22847–22857.
11. Ishii T, Itoh K, Takahashi S, Sato H, Yanagawa T, Katoh Y *et al* (2000) Transcription factor Nrf2 coordinately regulates a group of oxidative stress-inducible genes in macrophages. *J Biol Chem* **275**:16023–16029.
12. Johansen T, Lamark T (2011) Selective autophagy mediated by autophagic adapter proteins. *Autophagy* **7**:279–296.
13. Kabeya Y, Mizushima N, Yamamoto A, Oshitani-Okamoto S, Ohsumi Y, Yoshimori T (2004) LC3, GABARAP and GATE16 localize to autophagosomal membrane depending on form-II formation. *J Cell Sci* **117**:2805–2812.
14. Kahle PJ (2008) alpha-Synucleinopathy models and human neuropathology: similarities and differences. *Acta Neuropathol* **115**:87–95.
15. Kim OJ, Ariano MA, Namkung Y, Marinec P, Kim E, Han J, Sibley DR (2008) D2 dopamine receptor expression and trafficking is regulated through direct interactions with ZIP. *J Neurochem* **106**:83–95.
16. Komatsu M, Waguri S, Chiba T, Murata S, Iwata J, Tanida I *et al* (2006) Loss of autophagy in the central nervous system causes neurodegeneration in mice. *Nature* **441**:880–884.
17. Komatsu M, Waguri S, Koike M, Sou YS, Ueno T, Hara T *et al* (2007) Homeostatic levels of p62 control cytoplasmic inclusion body formation in autophagy-deficient mice. *Cell* **131**:1149–1163.
18. Komatsu M, Kurokawa H, Waguri S, Taguchi K, Kobayashi A, Ichimura Y *et al* (2010) The selective autophagy substrate p62 activates the stress responsive transcription factor Nrf2 through inactivation of Keap1. *Nat Cell Biol* **12**:213–223.
19. Kramer ML, Schulz-Schaeffer WJ (2007) Presynaptic alpha-synuclein aggregates, not Lewy bodies, cause neurodegeneration in dementia with Lewy bodies. *J Neurosci* **27**:1405–1410.
20. Kruger R, Kuhn W, Muller T, Woitalla D, Graeber M, Kosel S *et al* (1998) Ala30Pro mutation in the gene encoding alpha-synuclein in Parkinson's disease. *Nat Genet* **18**:106–108.
21. Lee MK, Stirling W, Xu Y, Xu X, Qui D, Mandir AS *et al* (2002) Human alpha-synuclein-harboring familial Parkinson's disease-linked Ala-53 –> Thr mutation causes neurodegenerative disease with alpha-synuclein aggregation in transgenic mice. *Proc Natl Acad Sci U S A* **99**:8968–8973.
22. Mak SK, McCormack AL, Manning-Bog AB, Cuervo AM, Di Monte DA (2010) Lysosomal degradation of alpha-synuclein in vivo. *J Biol Chem* **285**:13621–13629.
23. Masliah E, Rockenstein E, Veinbergs I, Mallory M, Hashimoto M, Takeda A *et al* (2000) Dopaminergic loss and inclusion body formation in alpha-synuclein mice: implications for neurodegenerative disorders. *Science* **287**:1265–1269.
24. Matsuoka Y, Vila M, Lincoln S, McCormack A, Picciano M, LaFrancois J *et al* (2001) Lack of nigral pathology in transgenic mice expressing human alpha-synuclein driven by the tyrosine hydroxylase promoter. *Neurobiol Dis* **8**:535–539.
25. Mazzulli JR, Xu YH, Sun Y, Knight AL, McLean PJ, Caldwell GA *et al* (2011) Gaucher disease glucocerebrosidase and alpha-synuclein form a bidirectional pathogenic loop in synucleinopathies. *Cell* **146**:37–52.
26. Nezis IP, Simonsen A, Sagona AP, Finley K, Gaumer S, Contamine D *et al* (2008) Ref(2)P, the *Drosophila melanogaster* homologue of mammalian p62, is required for the formation of protein aggregates in adult brain. *J Cell Biol* **180**:1065–1071.
27. Odagiri S, Tanji K, Mori F, Kakita A, Takahashi H, Wakabayashi K (2012) Autophagic adapter protein NBR1 is localized in Lewy bodies and glial cytoplasmic inclusions and is involved in aggregate formation in alpha-synucleinopathy. *Acta Neuropathol* **124**:173–186.
28. Okada K, Yanagawa T, Warabi E, Yamastu K, Uwayama J, Takeda K *et al* (2009) The alpha-glucosidase inhibitor acarbose prevents obesity and simple steatosis in sequestosome 1/A170/p62 deficient mice. *Hepatol Res* **39**:490–500.
29. Pankiv S, Clausen TH, Lamark T, Brech A, Bruun JA, Outzen H *et al* (2007) p62/SQSTM1 binds directly to Atg8/LC3 to facilitate degradation of ubiquitinated protein aggregates by autophagy. *J Biol Chem* **282**:24131–24145.
30. Paumier KL, Sukoff Rizzo SJ, Berger Z, Chen Y, Gonzales C, Kaftan E *et al* (2013) Behavioral characterization of A53T mice reveals early and late stage deficits related to Parkinson's disease. *PLoS ONE* **8**:e70274.

31. Polymeropoulos MH, Lavedan C, Leroy E, Ide SE, Dehejia A, Dutra A *et al* (1997) Mutation in the alpha-synuclein gene identified in families with Parkinson's disease. *Science* **276**:2045–2047.
32. Quan W, Kim HK, Moon EY, Kim SS, Choi CS, Komatsu M *et al* (2012) Role of hypothalamic proopiomelanocortin neuron autophagy in the control of appetite and leptin response. *Endocrinology* **153**:1817–1826.
33. Ramesh Babu J, Lamar Seibenhener M, Peng J, Strom AL, Kemppainen R, Cox N *et al* (2008) Genetic inactivation of p62 leads to accumulation of hyperphosphorylated tau and neurodegeneration. *J Neurochem* **106**:107–120.
34. Richfield EK, Thiruchelvam MJ, Cory-Slechta DA, Wuertzer C, Gainetdinov RR, Caron MG *et al* (2002) Behavioral and neurochemical effects of wild-type and mutated human alpha-synuclein in transgenic mice. *Exp Neurol* **175**:35–48.
35. Riley BE, Kaiser SE, Shaler TA, Ng AC, Hara T, Hipp MS *et al* (2010) Ubiquitin accumulation in autophagy-deficient mice is dependent on the Nrf2-mediated stress response pathway: a potential role for protein aggregation in autophagic substrate selection. *J Cell Biol* **191**:537–552.
36. Rockenstein E, Mallory M, Hashimoto M, Song D, Shults CW, Lang I, Masliah E (2002) Differential neuropathological alterations in transgenic mice expressing alpha-synuclein from the platelet-derived growth factor and Thy-1 promoters. *J Neurosci Res* **68**:568–578.
37. Rodriguez A, Duran A, Selloum M, Champy MF, Diez-Guerra FJ, Flores JM *et al* (2006) Mature-onset obesity and insulin resistance in mice deficient in the signaling adapter p62. *Cell Metab* **3**:211–222.
38. Seibenhener ML, Babu JR, Geetha T, Wong HC, Krishna NR, Wooten MW (2004) Sequestosome 1/p62 is a polyubiquitin chain binding protein involved in ubiquitin proteasome degradation. *Mol Cell Biol* **24**:8055–8068.
39. Settembre C, Di Malta C, Polito VA, Garcia Arencibia M, Vetrini F, Erdin S *et al* (2011) TFEB links autophagy to lysosomal biogenesis. *Science* **332**:1429–1433.
40. Singleton AB, Farrer M, Johnson J, Singleton A, Hague S, Kachergus J *et al* (2003) alpha-Synuclein locus triplication causes Parkinson's disease. *Science* **302**:841.
41. Spillantini MG, Schmidt ML, Lee VM, Trojanowski JQ, Jakes R, Goedert M (1997) Alpha-synuclein in Lewy bodies. *Nature* **388**:839–840.
42. Tanji K, Mori F, Mimura J, Itoh K, Kakita A, Takahashi H, Wakabayashi K (2010) Proteinase K-resistant alpha-synuclein is deposited in presynapses in human Lewy body disease and A53T alpha-synuclein transgenic mice. *Acta Neuropathol* **120**:145–154.
43. Tanji K, Zhang HX, Mori F, Kakita A, Takahashi H, Wakabayashi K (2012) p62/sequestosome 1 binds to TDP-43 in brains with frontotemporal lobar degeneration with TDP-43 inclusions. *J Neurosci Res* **90**:2034–2042.
44. Unger EL, Eve DJ, Perez XA, Reichenbach DK, Xu Y, Lee MK, Andrews AM (2006) Locomotor hyperactivity and alterations in dopamine neurotransmission are associated with overexpression of A53T mutant human alpha-synuclein in mice. *Neurobiol Dis* **21**:431–443.
45. van der Putten H, Wiederhold KH, Probst A, Barbieri S, Mistl C, Danner S *et al* (2000) Neuropathology in mice expressing human alpha-synuclein. *J Neurosci* **20**:6021–6029.
46. Webb JL, Ravikumar B, Atkins J, Skepper JN, Rubinsztein DC (2003) Alpha-Synuclein is degraded by both autophagy and the proteasome. *J Biol Chem* **278**:25009–25013.
47. Winder-Rhodes SE, Garcia-Reitbock P, Ban M, Evans JR, Jacques TS, Kemppinen A *et al* (2012) Genetic and pathological links between Parkinson's disease and the lysosomal disorder Sanfilippo syndrome. *Mov Disord* **27**:312–315.
48. Wooten MW, Geetha T, Babu JR, Seibenhener ML, Peng J, Cox N *et al* (2008) Essential role of sequestosome 1/p62 in regulating accumulation of Lys63-ubiquitinated proteins. *J Biol Chem* **283**:6783–6789.

SUPPORTING INFORMATION

Additional Supporting Information may be found in the online version of this article at the publisher's web-site:

Video Clip S1. The Morris water maze test. A wild-type mouse successfully reaches the platform within 30 s on the fourth day of training course.

Video Clip S2. The Morris water maze test. A p62-knockout mouse does not take an action within 60 s, and end up failing on the fourth day of training course.

PLOS ONE

Releasing Dentate Nucleus Cells from Purkinje Cell Inhibition Generates Output from the Cerebrocerebellum

Takahiro Ishikawa[1], Saeka Tomatsu[3], Yoshiaki Tsunoda[2], Jongho Lee[1], Donna S. Hoffman[4,5], Shinji Kakei[1]*

1 Motor Disorders Project, Tokyo Metropolitan Institute of Medical Science, Setagaya, Tokyo, Japan, **2** Frontal Lobe Function Project, Tokyo Metropolitan Institute of Medical Science, Setagaya, Tokyo, Japan, **3** Department of Neurophysiology, National Institute of Neuroscience, National Center of Neurology and Psychiatry, Kodaira, Tokyo, Japan, **4** Department of Neurobiology, University of Pittsburgh School of Medicine, Pittsburgh, Pennsylvania, United States of America, **5** Center for the Neural Basis of Cognition, University of Pittsburgh School of Medicine, Pittsburgh, Pennsylvania, United States of America

Abstract

The cerebellum generates its vast amount of output to the cerebral cortex through the dentate nucleus (DN) that is essential for precise limb movements in primates. Nuclear cells in DN generate burst activity prior to limb movement, and inactivation of DN results in cerebellar ataxia. The question is how DN cells become active under intensive inhibitory drive from Purkinje cells (PCs). There are two excitatory inputs to DN, mossy fiber and climbing fiber collaterals, but neither of them appears to have sufficient strength for generation of burst activity in DN. Therefore, we can assume two possible mechanisms: post-inhibitory rebound excitation and disinhibition. If rebound excitation works, phasic excitation of PCs and a concomitant inhibition of DN cells should precede the excitation of DN cells. On the other hand, if disinhibition plays a primary role, phasic suppression of PCs and activation of DN cells should be observed at the same timing. To examine these two hypotheses, we compared the activity patterns of PCs in the cerebrocerebellum and DN cells during step-tracking wrist movements in three Japanese monkeys. As a result, we found that the majority of wrist-movement-related PCs were suppressed prior to movement onset and the majority of wrist-movement-related DN cells showed concurrent burst activity without prior suppression. In a minority of PCs and DN cells, movement-related increases and decreases in activity, respectively, developed later. These activity patterns suggest that the initial burst activity in DN cells is generated by reduced inhibition from PCs, i.e., by disinhibition. Our results indicate that suppression of PCs, which has been considered secondary to facilitation, plays the primary role in generating outputs from DN. Our findings provide a new perspective on the mechanisms used by PCs to influence limb motor control and on the plastic changes that underlie motor learning in the cerebrocerebellum.

Citation: Ishikawa T, Tomatsu S, Tsunoda Y, Lee J, Hoffman DS, et al. (2014) Releasing Dentate Nucleus Cells from Purkinje Cell Inhibition Generates Output from the Cerebrocerebellum. PLoS ONE 9(10): e108774. doi:10.1371/journal.pone.0108774

Editor: Tim Douglas Aumann, Florey Institute of Neuroscience & Mental Health, Australia

Received June 17, 2014; **Accepted** August 24, 2014; **Published** October 3, 2014

Data Availability: The authors confirm that all data underlying the findings are fully available without restriction. All relevant data are within the paper.

Funding: This work was supported by the Tokyo Metropolitan Institute of Medical Science and grants-in-aid from the Japan Science and Technology Agency (PRESTO) to SK (http://www.jst.go.jp/) and from the Ministry of Education, Culture, Sports, Science and Technology in Japan (http://www.mext.go.jp/) (No. 14580784, No. 15016008, No. 16015212, No. 20033029, No. 21500319) to SK and (No. 24650224) to TI and (No. 18700492, No. 20700478) to ST. This project was also supported by NBRP "Japanese Monkeys" through the National BioResource Project of the MEXT Japan. The funders had no role in study design, data collection and analysis, decision to publish, or preparation of the manuscript.

Competing Interests: The authors have declared that no competing interests exist.

* Email: kakei-sj@igakuken.or.jp

Introduction

The cerebellum generates its vast amount of output to the cerebral cortex through the dentate nucleus (DN), especially in monkeys. In fact, nuclear cells in DN generate burst activity prior to limb movement [1,2,3,4,5,6,7], and inactivation of DN results in cerebellar ataxia, a destruction of finely coordinated movement [8]. There are three sources of inputs to DN that may contribute to generation of the burst activity: mossy fiber (MF) collaterals, climbing fiber (CF) collaterals and Purkinje cells (PCs). MF collaterals and CF collaterals provide excitatory inputs, but neither can explain the burst activity in DN. MF collaterals are exceptionally minor in DN [9,10,11,12,13,14], in striking contrast to the other cerebellar nuclei, i.e. the interpositus nucleus (IP) and the fastigial nucleus. Discharge of the CF (~1 Hz) is too infrequent to explain the burst activity of DN cells. The remaining inputs from PCs are even more enigmatic because they are inhibitory and exert tonic suppression of DN cells. To explain the cause of excitation of deep cerebellar nuclear (DCN) cells in general without effective excitatory drive, there are two proposed mechanisms. First, some researchers proposed recruitment of a post-inhibitory rebound excitation [15,16,17,18]. They observed a short burst of DCN cells after current-induced hyperpolarization or synchronous activation of a large number of PCs. However, there are vigorous discussions about whether the conditions required for rebound excitation are realistic in physiological conditions, especially in behaving animals [15,16,17,18,19,20]. Second, suppression of PC activity could generate burst activity of

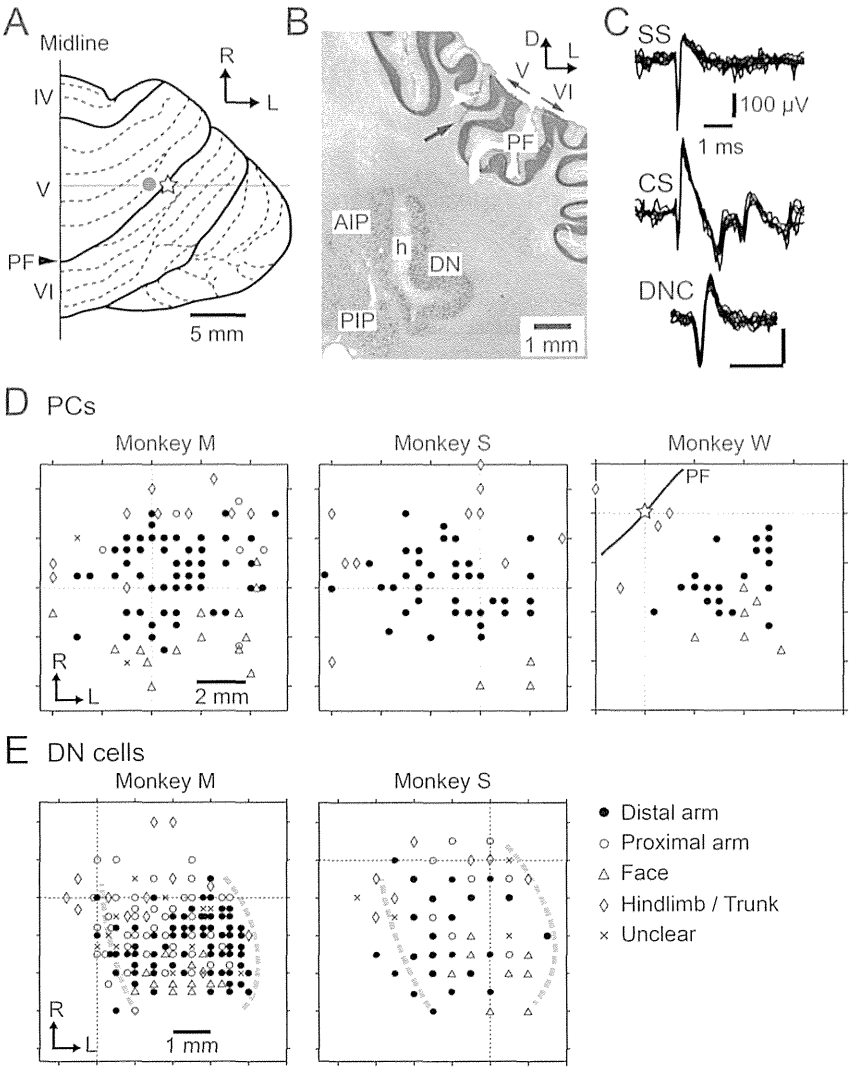

Figure 1. Recording sites of wrist-movement-related Purkinje cells (PCs) and dentate nucleus (DN) cells. A: Dorsal view of the right cerebellar hemisphere of monkey W. The open star indicates the center of the recording chamber. The gray dot marks the location of the electrolytic lesion indicated by the white arrowhead in B. PF: primary fissure, IV-VI: lobules IV-VI, R: rostral, L: lateral. B: Coronal section of the cerebellum of monkey W at the level of the gray line in A. The arrow indicates a recording track. The recording chamber was set at an angle to allow access to both the wrist-related cerebellar cortex and deep cerebellar nuclei (DCN). DN: dentate nucleus, AIP: anterior interpositus nucleus, PIP: posterior interpositus nucleus, h: hilum, D: dorsal, L: lateral. C: Typical examples of unit activities of simple spikes (SS, top) and complex spikes (CS, middle) for a PC and for a DN cell (DNC, bottom). D and E: Somatotopy maps of PCs for the three animals (D) and DN cells for the two animals (E). Cells with receptive fields (RFs) in distal arm (filled circles), proximal arm (open circles), face/mouth (open triangles) and hindlimb/trunk (open diamonds) are plotted. Note that all cells with RF in distal arm (filled circles) were task-related. In some cells, RF was unclear (cross marks). In D, the gray lines in the left (Monkey M) and middle (Monkey S) panels indicate locations of the PF. In the right panel (Monkey W), the open star and the PF (black line) correspond to those in A. The intersection of the two dashed lines indicates the center of the recording chamber in each animal. In E, the medial gray dashed line indicates the presumed medial edge of DN, whereas the lateral gray dashed line indicates the presumed lateral edge of DN. The medial border corresponds to the location of the axon bundle in the hilum of DN (indicated by *h* in B). The lateral border was estimated due to a lack of unit activities beyond the lines (See Materials and Methods). In both the cerebellar cortex and DN, recorded cells that had RFs in the face region were located caudal to the wrist-movement related cells, while cells that had RFs in the hindlimb/trunk were located rostrally.
doi:10.1371/journal.pone.0108774.g001

DCN cells by disinhibition, as suggested by previous studies [13,21,22,23,24]. Indeed, Heiney et al. [25] very recently demonstrated that a transient suppression of PC activity was capable of activating DCN cells.

To address how DN cells become activated during voluntary limb movements, we compared the temporal patterns of movement-related changes in activity for PCs and DN cells recorded from the same monkeys during step-tracking movements of the wrist. If rebound excitation works, phasic excitation of PCs and a concomitant inhibition of DN cells should precede excitation of DN cells. On the other hand, if disinhibition plays a primary role, phasic suppression of PCs and activation of DN cells should be observed at the same timing. We found that a great majority of PCs showed an initial suppression of their activity prior to movement onset, while a great majority of DN cells showed an initial facilitation without a preceding suppression. In a minority of PCs and DN cells, movement-related increases and decreases in activity, respectively, developed later. Our results suggest that a

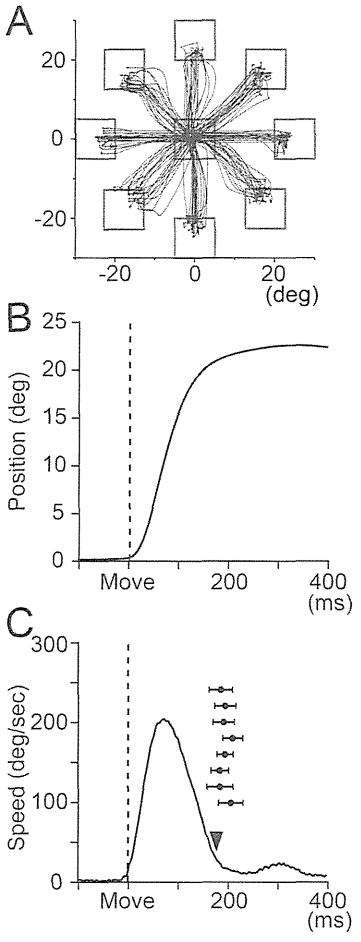

Figure 2. Movement kinematics of the wrist joint. A: Movement trajectories to 8 peripheral targets (10 trials for each target [square]) in the pronated forearm posture in monkey M. The target locations required 20° changes in the angle of the wrist joint. Each trace represents a single trial of movement. B: An example temporal profile of wrist angle (displacement) in a single trial. C: An example temporal profile of wrist speed in a single trial. Filled inverted triangle indicates the time of target acquisition (i.e., when the cursor moved into the target). Black circles with error bars indicate the mean ± SD of the time of target acquisition in eight movement directions (twenty trials each). Vertical dashed line labeled 'Move' indicates movement onset.
doi:10.1371/journal.pone.0108774.g002

decrease of inhibition from PCs, i.e., disinhibition, plays the primary role in activating DN cells. Our results further suggest that, contrary to our previous belief, suppression rather than facilitation of PCs plays the primary role in generating output from DN cells.

Materials and Methods

Ethics statement

All animal experimentation was conducted in accordance with the Guide for the Care and Use of Laboratory Animals (National Research Council. Washington, DC: National Academy Press, 1996) and the Guiding Principles for the Care and Use of Animals in the Field of Physiological Sciences (The Physiological Society of Japan, revised 2001). All surgical and experimental protocols were approved by the Animal Care and Use Committee of Tokyo Metropolitan Institute of Medical Science, and all efforts were made to minimize suffering.

We used three Japanese monkeys (*Macaca fuscata*, one female [monkey S] and two males [monkey M and monkey W], 6.0 kg, 8.0 kg and 7.8 kg, respectively). Animals were obtained through a government source (National BioResource Project "Japanese monkeys"). They received regular (on every weekday) veterinary checks. Each animal was housed in a cage specifically designed for macaques in an animal facility whose room temperature (18–23°C) and lighting (12-hour cycle) were controlled automatically. They were kept with other housed conspecifics and no other species. We provided animals chew toys as environmental enrichment in the cage. Animals were fed 150 g monkey biscuits once a day at 10 a.m. They also received fruit/vegetable pieces (total ~200 g) in the afternoon. When animals were not on water control, animals had unlimited access to water through a spigot at the front of the cage. When they were on fluid control, they received water everyday regardless of performance. Body weight was measured at least once each week and the animal was taken off study if the body weight dropped below 15% of the fully hydrated weight.

A recording chamber (30 mm in diameter) was implanted in a surgical room that was specifically designed for primates using aseptic techniques and full surgical anesthesia (Ketamine, 4 mg/kg IM. and xylazine, 0.5 mg/kg IM, followed by pentobarbital sodium, initial dose = 10 mg/kg IV, supplemented IM. as required). Animals were closely monitored prior to, during and after surgery until they could safely sit upright on their own. At the end of surgery, an analgesic was administered to the animals (Butorphanol, 0.1 mg/kg IM). The chamber was stereotaxically positioned on the hemispheric part of lobules V and VI of the cerebellum (Fig. 1A, B) ipsilateral to the trained (right) hand, based on magnetic resonance imaging (MRI). The target region was assumed to correspond to the area where arm-related PCs have been described previously [26,27,28,29]. In order to record wrist-related PCs and DCN cells within a single recording chamber, we tilted the chamber laterally by 40–45 degrees from the vertical. We obtained MRI images after surgery to identify the recording area in the cerebellum. For the MRI scan, the animal was anesthetized and monitored throughout the scan and during recovery from anesthesia.

In monkey W, a small electrolytic lesion (10 μA for 10 s) was made at selected sites in the cerebellar cortex (e.g. filled gray circle in Fig. 1A and white arrow head in Fig. 1B) near the end of the recording period. Then, the monkey was deeply anesthetized with a lethal dose (75 mg/kg, IV) of pentobarbital sodium before perfusion, and perfused with physiological saline followed by 10% formalin.

Task design of step-tracking movement of the wrist

Details of the task were described in Kakei et al. [30]. Briefly, monkeys sat in a primate chair with their forearm supported and grasped the handle of a manipulandum. The device rotated around the two axes of wrist joint motion: flexion-extension and radial-ulnar deviation. The monkeys faced an LCD monitor and moved a small cursor that moved in proportion to the animals' wrist movements. The monkeys began the task by placing the cursor inside the central target (Fig. 2A). After a variable hold period (0.8–1.2 s), a second target (open rectangle, 8° diameter) appeared at one of eight peripheral locations evenly spaced at 45° intervals on the screen. Following a variable instruction period (1–2 s), the central target was extinguished. This served as a 'GO' signal that indicated to the animals to move the cursor to the peripheral target. The animals were required to complete the initial movement within 0.5 s and hold the cursor within a peripheral target for at least 0.2 s. Target locations required a 20°

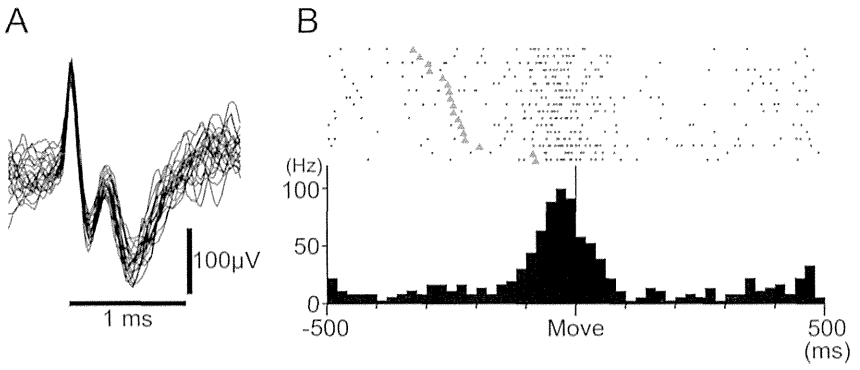

Figure 3. Movement-related activity of an example MF. A: A typical example of unit activity of a MF recorded at the location where task-related PCs were recorded. B: Movement-related activity of MF in A. Rasters and histogram are aligned on movement onset (Move), indicated by the solid line in the center of the histogram. Filled gray triangles in the rasters indicate the Go cue. Rasters are sorted by the timing of Go cue. Histogram bin width = 20 ms. Similar to this example, most MFs showed a strong movement-related increase in unit activity that started before movement onset. However, onset time, duration and depth of modulation differed in each direction and among MFs.
doi:10.1371/journal.pone.0108774.g003

change in wrist angle. After 0.5 s of reaching the target, the animal obtained a drop of juice as a reward. The eight targets were presented in a randomized block design. The monkeys performed the task with the forearm in the fully pronated and/or supinated positions. Monkeys' performance was quite stable in terms of both movement kinematics (Fig. 2) and percentage of correct trials (> 90%).

Extracellular recordings and identification of cerebellar neurons

We recorded neural activity with glass-coated Elgiloy electrodes (0.8–1.8 MΩ). In order to make recordings from the deep portion of the cerebellum, we used a customized microdrive with a 40 mm range of drive (MO-95S, Narishige, Japan). We used conventional techniques to make extracellular recordings of unit activity of single cells in the hemispheric part of the cerebellar lobules V/VI and in DCN. Single unit activities were amplified (x 10,000) and band-pass filtered (150–30,000 Hz) by an amplifier (AB-611J, Nihon-Kohden, Japan), isolated with a Multi Spike Detector (Alpha Omega, Israel), and then recorded along with movement kinematics at 1 kHz for both online and offline analysis. During recordings, isolated spike waveforms of recorded cells were sampled at 20 kHz. For each cell, we recorded 5–20 trials of data for each of 8 directions in one or more forearm postures.

When an electrode penetrated the tentorium cerebelli, activities of a number of putative PCs suddenly emerged. We searched for the most superficial layer of the cerebellar cortex where background noise disappeared, and considered this point as the surface of the cerebellar cortex. The depth from this point was used as a reference to identify PCs or DCN cells. PCs were identified by their location in the cerebellar cortex and the coexistence of characteristic simple spike (SS) and complex spike (CS) [27] (Fig. 1C). The occurrence of the SSs and the CSs in the same PC was identified by a silent period (>10 ms) of SSs after each CS [27,31]. In the cerebellar cortex, activities of MFs also were recorded [32]. MF activity was identified based on their characteristic spike waveform (Fig. 3A). Because the negative after-wave represents an excitatory postsynaptic potential in granule cells (GCs) [33], it is highly likely that we recorded the MF spikes near glomeruli. To record DCN cells, we used two criteria: 1) appropriate separation from the cerebellar cortex; 2) characteristic spike waveform. After passing through the last granular layer, we advanced the electrode through the subcortical white matter for an appropriate distance (>1500 μm) before encountering cells located at edges of IP or DN (cf. Fig. 1B). The putative DCN cells were usually clustered, and they demonstrated large negative-positive spikes (e.g. Fig. 1C, DNC) with initial negativities that were usually broader than those of PCs (e.g. Fig. 1C, SS and DNC). We also required that no cells in the cluster had spike waveforms like those of PCs, MFs, or any other cell type in the cerebellar cortex. It was usually possible to distinguish between DN and IP due to the existence of the axon bundle in the hilum of DN (Fig. 1B, *h*), where we found only small positive-negative axon spikes and relatively silent background activities. In monkeys M and S, the 3-dimensional distribution of putative DN cells corresponded well with the shape of DN confirmed in monkey W by histological reconstruction. In monkey W, a small electrolytic lesion (10 μA for 10 s) was made at selected sites in the cerebellar cortex (e.g. filled gray circle in Fig. 1A and white arrow head in Fig. 1B) near the end of the recording period. The monkey was deeply anesthetized with a lethal dose (75 mg/kg, IV) of pentobarbital sodium before perfusion, and perfused with physiological saline followed by 10% formalin. After post-fixing in 30% sucrose with 10% formalin, we prepared frozen-sections of the cerebellum (50 μm thick).

Examining receptive fields (RFs) of recorded cells

After recording unit activities, we examined the peripheral RFs of recorded cells. We used passive movements, palpation or brushing of the fingers, forearms, upper arms, shoulders, neck, chest, abdomen, back, face, and leg on both sides of the body to search for somatosensory afferent input. When a cell was activated by at least one of these stimuli, we considered the cell to have a somatosensory RF. We also searched for visual responses to directional movements of the examiner's hand in front of the animal or approach of the examiner's hand toward the animal's body. In addition, we checked whether the cells became active when the animals moved their wrist voluntarily.

Data analysis

We analyzed the recorded data with custom-made programs on MATLAB (MathWorks, USA). To detect movement onset, we set a threshold of movement speed at 15 degrees/s for each trial. We defined the mean discharge rate before the instruction signal (−500 to 0 ms relative to the instruction signal) as the spontaneous activity level. For each recorded cell, we compared the mean